EFFECT OF TEXTURE ON FORMABILITY AND MECHANICAL ANISOTROPY OF A SEVERE PLASTICALLY DEFORMED MAGNESIUM ALLOY

A Thesis

by

SONIA MODARRES RAZAVI

Submitted to the Office of Graduate Studies of
Texas A&M University
in partial fulfillment of the requirements for the degree of

MASTER OF SCIENCE

December 2011

Major Subject: Mechanical Engineering

Effect of Texture on Formability and Mechanical Anisotropy of a Severe Plastically Deformed Magnesium Alloy

EFFECT OF TEXTURE ON FORMABILITY AND MECHANICAL ANISOTROPY OF A SEVERE PLASTICALLY DEFORMED MAGNESIUM ALLOY

A Thesis

by

SONIA MODARRES RAZAVI

Submitted to the Office of Graduate Studies of
Texas A&M University
in partial fulfillment of the requirements for the degree of

MASTER OF SCIENCE

Approved by:

Chair of Committee,	Ibrahim Karaman
Committee Members,	Karl T. Hartwig
	Rashid K. Abu Al-Rub
Head of Department,	Jerald A. Caton

December 2011

Major Subject: Mechanical Engineering

ABSTRACT

Effect of Texture on Formability and Mechanical Anisotropy of a Severe Plastically Deformed Magnesium Alloy. (December 2011)

Sonia Modarres Razavi, B.S., Ferdowsi University of Mashhad, Mashhad, Iran

Chair of Advisory Committee: Dr. Ibrahim Karaman

Magnesium and its alloys have been considered as alternatives to aluminum alloys and steels for structural applications in automotive and aerospace applications due to their superior specific strength and light-weight. However, they have hexagonal-close packed (hcp) structure, and thus have a small number of deformation systems resulting in low ductility and formability near room temperature, anisotropic thermo-mechanical response and strong deformation textures. The aim of this work is to investigate experimentally the effect of crystallographic texture generated during severe plastic deformation (SPD), on the subsequent formability and mechanical flow anisotropy in AZ31B Mg alloy. The proper control of grain size and texture through SPD is expected to result in better low temperature formability and better control of mechanical flow anisotropy.

AZ31B Mg alloy has been successfully processed using equal channel angular extrusion (ECAE) following different processing routes, multiple passes, and different processing temperatures, in order to obtain samples with a wide variety of grain sizes, ranging from ~370 nm up to few microns, and crystallographic textures. Low

temperature processing of the AZ31B Mg alloy was successful after initial high temperature processing. Smaller grain sizes were achieved using the temperature step-down method leading to incremental reduction in grain size at each ECAE pass. The temperature step-down method was utilized to develop hybrid ECAE routes to obtain specific crystallographic textures. Optimized hybrid ECAE routes were developed which resulted in a high strength/high ductility material with the average grain size of ~370 nm. The ECAE processed alloy showed a high tensile yield strength of ~380 MPa that has never been reported so far in AZ31 ingot metallurgy Mg alloys.

The influence of grain size on the critical stress for the activation of individual deformation mechanisms was also investigated by systematically controlling the texture and grain size, and assuming the activation of mainly a single deformation mechanism through the careful selection of the loading direction on the processed samples. It was revealed that the Hall-Petch slope for the basal slip was much smaller than those of prismatic slip and tensile twinning.

To my wonderful parents, Farzaneh and Reza, my amazing sister, Sara, my great brother-in-law, Mahziar and my lovely and supportive husband, ***Navid****.*

ACKNOWLEDGEMENTS

First, I would like to thank my adviser, Dr. Karaman, who guided me in every step of this great achievement and without his guidance this mission would not have been accomplished.

I also thank Dr. Karaman's previous student, Dr. Majid Al-Maharbi, who taught me valuable research-related information and introduced me to the ECAE world. I thank my dear colleague and friend, David Foley, for his help and effort in this project. Mr. Robert Barber, who helped me a lot in processing the materials, and his patience and kindness are much appreciated.

I would like to thank my advisory committee, Dr. Hartwig and Dr. Abu Al-Rub, for their support and valuable comments. Dr. Duygulu's assistance in TEM imaging and specimen preparation is much appreciated. I am also thankful to Dr Karaman's group members, Pinar Karpuz, Nevin Ozdemir, Can Atli, Ebubekir Dogan, Ruixian Zhu, James Monroe, Ji Ma, Alper Evirgen, Murat Kaynak, Ankush Kothalkar, Cengiz Yegin, Li-Wei Tseng and Brian Franco, not only for the time they spent helping me in the lab, but also for being like family to me.

Last but not least, this work would not have been completed without the unconditional support of my husband, Navid Abedini; my wonderful mother, Farzaneh, for whom words cannot express my gratitude; my dearest father, Dr. Reza Modarres Razavi, who is the greatest role model for me and has always shown me the path to

success and my one and only sister, Sara, who always encourages me in all aspects of life.

TABLE OF CONTENTS

Page

CHAPTER Page

LIST OF FIGURES

FIGURE Page

FIGURE Page

FIGURE Page

FIGURE Page

LIST OF TABLES

TABLE Page

CHAPTER I

INTRODUCTION

1.1 Motivation

Magnesium alloys are of interest in aerospace, electronics, and particularly in the automotive industry due to their lightweight and high specific strength [1]. But at present, the applications of these alloys are still limited as compared to aluminum alloys. The reason lies in the fact that magnesium and its alloys have hexagonal-close packed (hcp) structure. This structure, unlike cubic structures, does not have enough number of independent slip systems to accommodate plastic deformation, which results in poor ductility and formability near room temperature [2, 3]. Moreover, because of the large difference between the critical resolve shear stresses (CRSS) of different slip systems, these alloys tend to have strong deformation textures and highly anisotropic mechanical properties [4-6]. In some applications, highly anisotropic deformation can give these alloys an advantage over other more isotropic structural materials, such as in blast protection applications.

To overcome some of the limitations of Mg alloys, several processing techniques have been utilized [7-9].

This thesis follows the style of Scripta Materialia.

One such processing technique is equal channel angular extrusion (ECAE) which has been extensively used to increase the strength and ductility of many materials by refining the microstructure and also controlling the crystallographic texture via severe plastic deformation (SPD). By knowing that the crystallographic texture and grain morphology influence the mechanical response of the materials, we propose to use ECAE as the processing method because it is a promising technique which permits the application of high uniform strains without considerable change in the shape of the processed material. Moreover, deformation following different strain paths and applying multiple passes are possible with this technique.

The purpose of this study is the SPD of AZ31B (2.5-3.5 wt.% Al, 0.7-1.3 wt.% Zn, 0.2 wt.% Mn and balance Mg) starting at 200 °C followed by different routes to get advantage from dynamic recrystallization (DRX) and create specific crystallographic textures. The effect of each crystallographic texture on the mechanical response needs to be investigated.

There are few research groups that were able to ECAE process AZ31B Mg alloy at low temperatures, but they all did not explain thoroughly the reason behind the selection of the conducted hybrid ECAE route. Thus, a systematic study is required to fully understand how to improve the formability and control the mechanical flow anisotropy at low temperature ECAE processing. We utilize the temperature step-down method followed by different routes and number of passes to produce ultrafine-grained (UFG) AZ31B due to the suppression of DRX and added ECAE passes.

To the best knowledge of the author, no systematic results have been reported on the grain size dependency on the activation of individual deformation mechanisms. In order to activate a certain deformation system under loading along a particular direction, the control of the crystallographic texture and grain size during the ECAE processing was considered.

1.2 Statement of Objectives

The objectives of this work can be summarized as follows:

1. SPD processing of AZ31B alloy using ECAE following different processing routes, temperatures and up to different number of ECAE passes, utilizing temperature step-down method to develop hybrid ECAE routes with distinct crystallographic textures.
2. Find the best processing recipe, which includes the selection of routes, passes, processing temperature, and resulting texture, to obtain a high strength/high ductility AZ31B Mg alloy by ECAE processing.
3. Systematically investigate the feasibility of ECAE processing of AZ31B Mg alloy at low temperatures and evaluate its effects on room temperature mechanical properties.
4. Reveal the effect of texture on the formability of the AZ31B Mg alloy that has already been SPD processed.
5. Study the effect of grain size on the activation of different deformation mechanisms in AZ31B Mg alloy.

CHAPTER II

LITERATURE REVIEW

2.1 Equal Channel Angular Extrusion (ECAE)

Grain refinement has long been utilized as a method of strengthening metals and alloys. Normally this can be accomplished through the use of traditional techniques like *rolling*, *forging* and *extrusion*. But all these techniques result in reduction of cross-sectional area that occurs during processing. Although large values of strain can be applied, the finished product will be in the form of very thin foils or wires that have limited applications. ECAE processing is a method of inducing SPD in a material without reducing the cross-sectional area of the work-piece [10]. As the metal is forced through the angled die, large deformation and pressure are created. This massive deformation causes very different mechanical properties in different materials depending on a number of processing factors. The first experiments with ECAE were performed by Segal et al. [11, 12] during the 1970s and 1980s at the Physical Technical Institute Academy of Sciences of Buelorussia, Minsk in the former Soviet Union. The objective was to create large deformations in metal billets with simple shear as a metal forming method, rather than enforcing primarily pure shear like the common processes of rolling or conventional extrusion [13-17]. The initial research, while successful, received little attention until the 1990s when ECAE began to be heavily researched due to the UFG structures and the unique material properties that could be produced [11, 13, 18-21]. The first major report on the UFG structures resulting from ECAE showed up in the

International Symposium on Plasticity of Metals and Alloys (ISPMA-5), 1990, Prague. Valiev et al. [17] revealed research on a Mg alloy that displayed "unusual mechanical behavior" after undergoing an ECAE type procedure [14, 17].

Since then, the ECAE process itself has become more refined, as researchers have found methods to change how SPDs are applied. For instance, multiple passes are now made, ranging from one to sixteen, among which four commonly used routes are labeled A, C, B_A and B_C [15, 22]. It has been found that the grain structure and the properties are highly dependent on the chosen path and the angles of the die, around which the billet is forced [22].

Figure 2.1 depicts the components of the ECAE process. A billet is formed to fit exactly within a channeled die with an angled turn. The die is usually lubricated, in order to reduce possible frictional effects on the metal billet at the interface between the billet and the die walls. A plunger is used to press (or extrude) the billet through the angled die at lower working temperatures to create extremely large simple shear stresses without changing the cross-sectional area of the billet. Changing the route, by rotating the billet, changes the strain path during deformation. This results in some changes in the grain structure and material properties [23]. Among numerous routes, that have been tested, four routes have become commonly used and are shown in Figure 2.2.

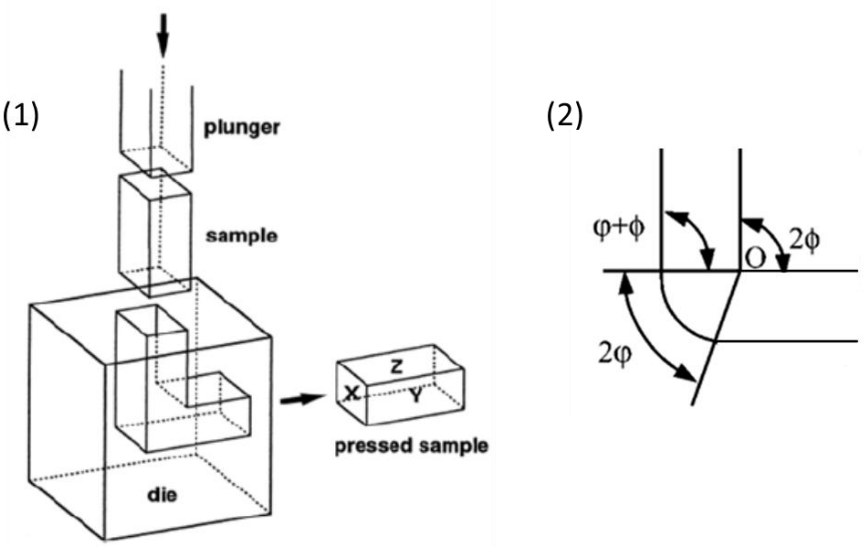

Figure 2.1 (1) Schematic of ECAE (ECAP) [24], (2) Schematic demonstrating the simple shear that the representative material element goes through during the process. 2ϕ is the die angle and 2ψ is the curvature angle ranging from 0°, for sharp die, and 90°[25].

Route A is the least complicated one, because it uses multiple passes through the die without any changes to the orientation of the billet. Route B_A also uses a 90° angled die, but the billet is rotated 90° back and forth before each pass is made. Route C rotates the billet 180° along the axial axis before each pass and route B_C rotates the billet 90° in the same direction (either clockwise or counter-clockwise) before each pass through the 90° angle die [26]. While the first three routes, A, B_A and C, achieve formation of UFG and high angle grain boundaries, experiments have shown, they are not as effective as the B_C route at doing so [26-28]. The effectiveness of the B_C route is explained by three factors dealing with the shearing stress patterns: (i) the shearing takes place over larger angular ranges, (ii) the original orientation is used after every fourth pass, and (iii) there is deformation on all three planes [27].

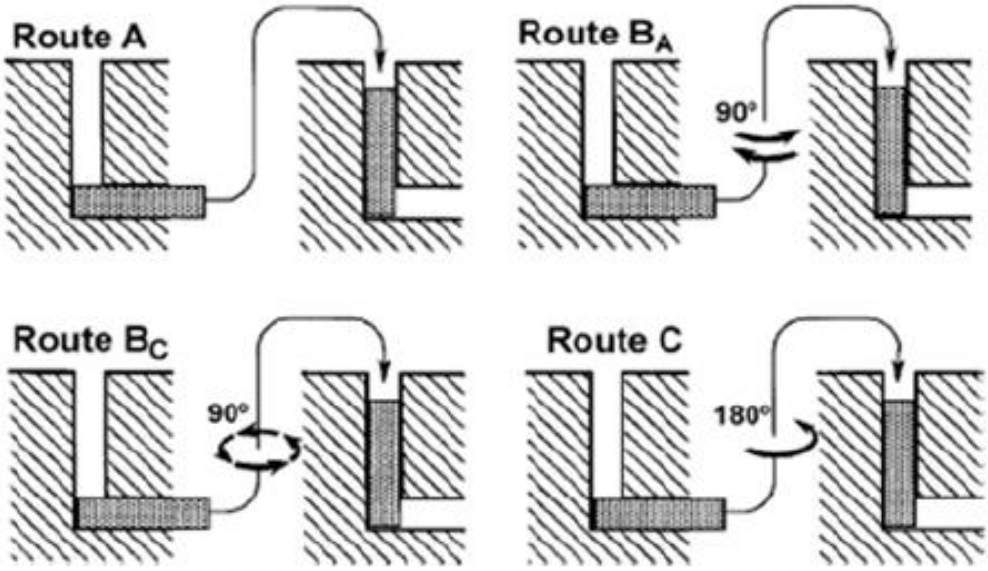

Figure 2.2 The four most common routes in ECAE [14].

While these are the most common routes, there are still other well-known routes such as E. Route E consists of a 180° rotation of the billet after the initial pass followed by a 90° rotation in the same direction between pass two and pass three. The process is then repeated with 90° rotations occurring before every even numbered pass [29].

Changing the orientation of the billet changes the slip systems, which are activated by the shear stresses as the sample is forced around the internal angle [13]. Activating different slip systems leads to different properties and texture of the material. The internal angle of the die is the most critical factor in controlling the level of the strain, imposed on the metal billet. On the other hand, the external angle of curvature has some minor effects on the strains. Some groups argued that having a die with a round corner will introduce an increase in the extent of inhomogeneities in the as-pressed

billets [30, 31], but Valiev et al. [13] claim that the most promising approach is to construct a die with a channel angle of 90°, with an outer angle of curvature 20° and with no arc of curvature at the inner point of intersection of the two parts of the channel.

In the ECAE process, if the two channels are intersected at an angle 2φ, the effective Von Mises strain per pass can be calculated using the following equation [12, 32]:

$$\varepsilon = \frac{2}{\sqrt{3}} \cot \varphi$$

The accumulated strain after multiple passes (N) is calculated by multiplying the strain value from the above equation by N. In the case of dies having arcs of curvature as seen in Figure 2.1 (2), the equivalent strain for N number of passes is determined as follows [33]:

$$\varepsilon = \frac{N}{\sqrt{3}} [2 \cot(\varphi + \psi) + \psi \csc(\varphi + \psi)]$$

where, ψ is the angle outlined by the arc of curvature at the point of intersection. The equations above are based on the ideal deformation situation, which reveal the deformation mechanisms in the process [25]. But in reality there are many factors that influence the material flow and deformation mechanisms during ECAE. These factors can be the *friction* between the billet and ECAE die, *deformation temperature*, *strain rate*, *dynamic material properties*, and *thermal behaviors* of the material being deformed. Much more advanced modeling through FEM is necessary for better simulating the actual changes in the strains and properties of the material. For typical dies, with the channel angle of 90°, the equivalent strain is close to one for a single pass,

and this strain is independent of the arc of curvature [13]. Nakashima et al. [34] reported that although it is easier to achieve a large plastic strain by pressing the material through a die, with a large internal angle, but a UFG structure with high angle grain boundaries may be achieved most readily by imposing a very intense plastic strain on the sample through the die with an internal angle close to 90°.

Through numerous speed tests with aluminum, it has been shown that the equilibrium grain size does not change significantly with the speed that the plunger forces the billet through the die [13, 26]. However, speed can affect the temperature at which extrusion can take place and research cited by Valiev et al. [13] has also shown that processing at slower speeds will produce "more equilibrated microstructures" [20, 35, 36]. Therefore, hydraulic presses are commonly used to control the speed and the processing time.

Processing temperature and internal heating from friction do affect the grains formed during processing. Experiments have shown that the grain size and the fraction of low angled grain boundaries increase in the metals processed at higher temperatures [26]. In an ECAE process, the goal is to create UFG materials. Processing metals by extrusion at higher temperatures is considerably easier. Also we need to ensure that the lowest friction occurs between the die and the billet. Hence, it is necessary to process the billets at the lowest possible extrusion temperature, in order to reduce thermal effects. Because stronger materials can generate more internal heat from the processing, they will not deform as easily. Thus, the walls of the die should be properly lubricated before trying to process a metal billet. Also, each pass through the die removes the layer of

lubrication. Therefore it is necessary to re-lubricate the die walls and the billet before passes [37].

Other than advantages mentioned above, ECAE can be used on a wide range of billet sizes, including large enough billets, used for structural applications [13, 22]. At sufficient strains, the procedure is capable of controlling crystallographic texture and refining the microstructure of the material, which can help reduce the anisotropy [29, 38]. However, this requires a near frictionless die with sharp inner and outer corners and if this is not the case, the material will be heterogeneous along its longitudinal axis [38].

ECAE processing offers many advantageous changes to the material properties and grain structure of metals. These types of property changes result in much higher strength values in smaller grained, especially UFG, materials when compared to coarse grained materials that resulted from common metal processing techniques [13].

2.2 Magnesium Alloys

The plastic deformation of Mg and its alloys is accommodated mainly by the glide of <a>-type dislocations on (0001) basal and $\{10\bar{1}0\}$ prismatic planes, the glide of $\langle c+a\rangle$-type dislocations on $\{11\bar{2}2\}$ pyramidal planes, $\{10\bar{1}2\}$ extension and $\{10\bar{1}1\}$ contraction twinning [39]. According to Taylor [40] and von Mises [41], there should be five independent slip systems for a polycrystalline material to be able to undergo a homogenous deformation. Basal <a> and prismatic <a> slips consist of only four independent slip systems in Mg alloys. Although pyramidal <a> has four independent modes, this is crystallographically equivalent to the cross slip between basal and

prismatic systems [42]. Pyramidal <c+a> has five independent modes and it can fulfill the Taylor criterion by itself, but $\{11\bar{2}2\}$ plane is associated with the largest Burgers vector, the smallest interplanar spacing and thus the hardest "ease of gliding" [42]. This makes its CRSS much higher compared to that of basal slip. According to some previous reports on Mg single crystals, the CRSS of a basal slip system, at room temperature, is approximately 1/100 of that of non-basal slip systems on prismatic and pyramidal planes [43, 44].

Other than the deformation caused by slip along crystallographic planes, deformation twinning is also an important mechanism for hcp metals. Depending on whether twinning results in an elongation or reduction of the c-axis length, there are two types of twinning in Mg alloys: $\{10\bar{1}2\}\langle 10\bar{1}1\rangle$ *tensile* or $\{10\bar{1}1\}\langle 10\bar{1}2\rangle$ *compressive*. The activation of each of these mechanisms depends on the material, the temperature, and the strain rate [45]. In Figure 2.3, the most active deformation modes in Mg alloys are presented schematically. At room temperature, the two dominant deformation modes of Mg alloys are basal slip and $\{10\bar{1}2\}\langle 10\bar{1}1\rangle$ twinning [20]. As temperature rises the activation of non-basal slips is more possible due to lower CRSS; thus a better formability can be resulted [46]. According to Yoo [42], depending on the c/a ratio, the twinning modes may be either tensile or compressive. The critical value of this ratio is $\sqrt{3}$, which makes the shear plane a square and the twinning shear becomes zero. If the c/a ratio is less than 1.633, $\{10\bar{1}2\}$ twin helps to extend along the c-axis, and thus it is

called tensile twin, as the case in magnesium. $\{10\bar{1}2\}$ tensile twinning causes the basal pole to be reoriented by ~86° [47, 48].

In large-grained Mg alloys, twinning is observed from the early stage of plastic deformation and actually serves as an additional deformation mechanism to satisfy von Mises criterion. On the other hand, it was shown that in a fine-grained AZ31 alloys there was no noticeable twinning after 2% and some twinning was seen after deformation of 16% [49].

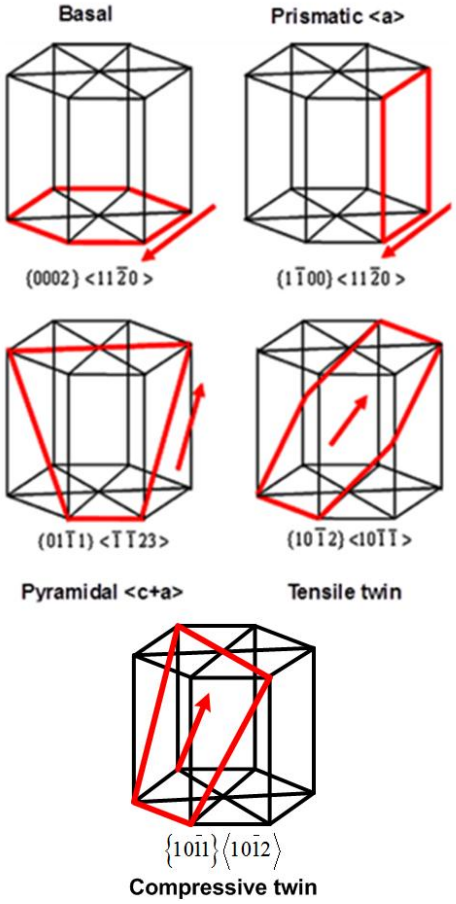

Figure 2.3 Five most active deformation modes in magnesium alloys [50].

Therefore, there must be additional dislocation mechanisms to replace twinning. Further investigations revealed that the yield anisotropy value changed from 100 to 1.1 in the fine-grained Mg alloy and this caused the activation of non-basal slips. For estimating the yield anisotropy the following relation is used:

$$\frac{\mu_{NBS}}{\mu_{BS}} = \frac{\tau_{NBS}}{\tau_{BS}}$$

Here, τ is the critical resolved shear stress; and μ is the Schmid factor, which is related to the orientation of a grain with respect to the direction of the applied stress. NBS and BS refer to non-basal slip system and basal slip system, respectively. The activity of non-basal slip was attributed in terms of grain-size dependent compatibility stress at grain boundaries [49].

2.3 Crystallographic Texture

According to Dr. Irene Beyerlein of Los Alamos National Laboratories, "Texture is defined as a microstructural property that describes the orientation distribution of the grains constituting a polycrystalline aggregate" [16]. Texture orientation can lead to highly anisotropic mechanical properties. This means that the material can be relatively strong (but brittle) when tested in one direction, but low in strength (and relatively ductile) when tested in another direction. This phenomenon has been seen even in weakly textured pure metals such as copper. ECAE process has created significant plastic anisotropy and tension/compression (T/C) strength asymmetry in the experiments on copper [51, 52].

The texture of Mg generated after rolling or conventional extrusion is well known. For the extruded Mg, basal planes are aligned with the extrusion axis and there is a tendency for the $\langle 10\bar{1}0 \rangle$ directions to align with the extrusion axis (figure on page 18). Hot-rolled Mg has basal poles parallel to the normal direction (figure on page 29). As for ECAE, different processing routes (A, B_C, B_A, C, etc.) have different strain paths resulting in different textures [20]. By knowing the texture of a material, the prediction of the mechanical response along different directions is possible. Thus, one can use texture evolution as a tool to control the mechanical properties of the material. In the present work, the crystallographic texture was an important factor that was taken into account for the selection of the routes.

There are many factors that influence the texture development, namely, the initial texture of the material, the active deformation mechanisms and deformation conditions, which themselves depend on die angle, number of passes and chosen route [15, 53]. A slight change of any of these factors can lead to large differences in the final texture.

2.4 Equal Channel Angular Extrusion of Magnesium Alloys

There have been many investigations and efforts in enhancing the mechanical properties of Mg alloys, in order to make them suitable for structural components. As explained in section 2.1, ECAE has been a good solution to enhance both strength and ductility in different materials, including Mg alloys, by reducing the grain size [17, 34, 35, 54-58]. However, in some cases (e.g. [59]) lower yield stresses were reported after

the ECAE process. The authors believed that the change in texture during ECAE was responsible for this result.

Various processing parameters such as processing routes, processing temperature and extrusion passes have an important influence on room temperature mechanical properties of processed materials by ECAE [36, 55, 60, 61].

It is well known that ECAE of hcp metals is conducted at elevated temperatures, because of the restricted number of deformation systems and poor formability [62, 63]. For pure Mg, the ECAE temperature increased to 400 °C to avoid fracturing [55]. This temperature is within the range where CRSS for the prismatic slip decreases appreciably and approaches that of the basal slip [64]. Addition of aluminum, e.g. in AZ31B, decreases the activation temperature for the prismatic slip or other pyramidal slips. Thus, it is reported that the lowest temperature, at which successful extrusions can occur and also grain refinement can be seen, is in the range of 200 °C-300 °C for AZ31B [20, 54].

Enforcing a back pressure by a second ram and hydraulic cylinder on the exit channel is very important during ECAE processing. Having back pressure prevents serious shear failure and it has been shown that the application of back pressure eliminates any gaps between the specimen and the die. This changes the mode of deformation to a simple shear. Having back pressure can also help processing at lower temperatures, thus resulting in a finer microstructure [35]. Agnew et al. [62] reported unsuccessful ECAE processing on AZ31B at lower temperatures (175 °C) even with back pressure. But they specified that by resisting the motion of the moveable ECAE die floor, shear failures can be eliminated [35]. A recent study by Ding et al. [36] argued

that by reducing the extrusion speed, multiple processing is possible at lower temperatures.

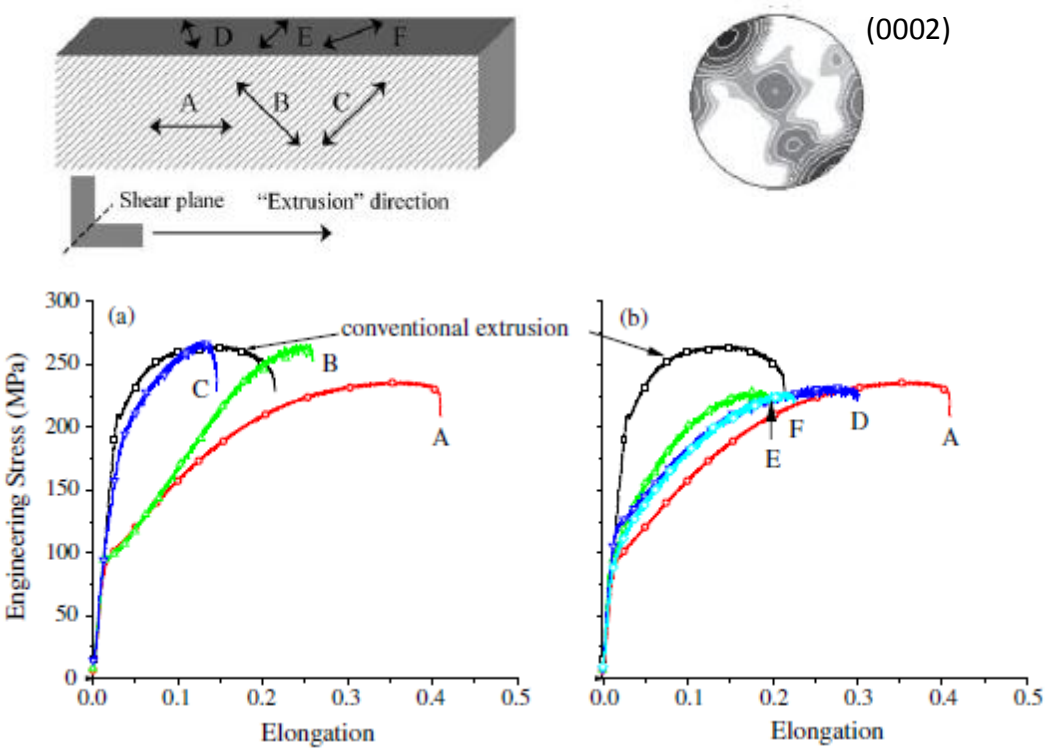

Figure 2.4 Engineering stress-strain results from AZ31 ECAE processed samples with various orientations showing flow stress anisotropy [35].

Agnew et al. [35] investigated the effects of texture on the flow stress anisotropy of AZ31B, processed by ECAE, by running tensile tests along various billet orientations (Figure 2.4). They found that the flow response is highly anisotropic, and this can be rationalized by the strong crystallographic texture, induced during ECAE. This study, however, was carried out only on a sample processed up to 8 passes via route B_C. Later, they carried out experiments on different Mg alloys such as AZ31B, ZK60, WE43 and

MgLi, to investigate the texture evolution during ECAE for each case. Figure 2.5 shows (0002) and $(10\bar{1}0)$ pole figures of these alloys that underwent up to four passes of ECAE following route A. From these textures, one can extract information about the relative activities of the deformation mechanisms, which accommodate the plastic deformation. For instance, AZ31B was deformed mainly by basal slip. The change in texture for ZK60 and WE43, compared to AZ31B, can be explained by the significant contribution from the non-basal slip mechanism [62].

It is important to note that Mukai et al. [54] and Agnew et al. [35] have annealed the ECAE processed samples to increase the grain size to that of as-conventionally extruded samples. This annealing resulted in high improvement in ductility.

In most of the studies, ECAE processing of Mg alloys was carried out at temperatures of 200 ^{o}C or above, which for Mg with sufficiently high homologous temperatures can potentially trigger DRX. DRX occurs most readily in materials in which recovery is slow, e.g., in materials of medium or low stacking fault energy (SFE) [65-67]. In magnesium, the SFE for basal, prismatic and pyramidal planes is ~36 mJ/m^2, ~265 mJ/m^2 and ~344 mJ/m^2, respectively [68]. Jiang et al. [60] carried out six-pass ECAE at route B_C on Mg-9Al-1Zn and found out that optimum room temperature mechanical properties exist with elevated processing temperature due to the increase in DRX. However, when the processing temperature rises from the "optimal temperature," coarsening occurs in the ECAE process, resulting in lower yield and ultimate strengths.

Some previous works [69-71] showed that it is necessary to process Mg alloys at low temperatures to suppress DRX, after high temperature ECAE processing. This will

prevent dynamic recovery and DRX and also preserve dislocations within the grains and at the grain boundaries. One can conclude that DRX is undesirable for achieving high yield strength in Mg alloys because it leads to new strain-free grains. However, producing these fine grains enhances the strength of the material at early stages of ECAE processing and before further processing at lower temperatures [72].

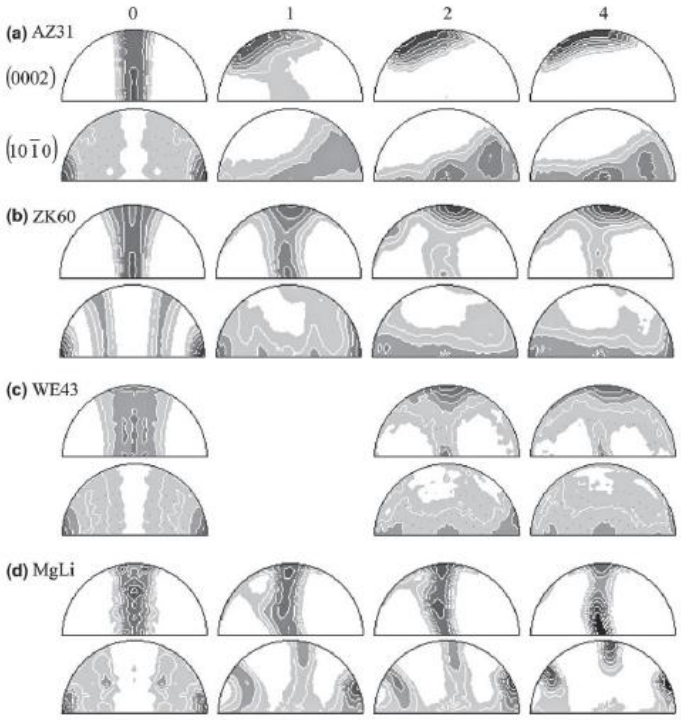

Figure 2.5 (0002) and $(10\bar{1}0)$ pole figures (upper half) show the initial extrusion textures (labeled 0) and ECAE textures after 1, 2, and 4 passes by route A [62]. All of the alloys were initially as-extruded.

Recently, a multiple-temperature processing of AZ31B by Ding et al. [36] consisted of four sequential steps: (1) 200 ^{o}C for four passes; (2) 150 ^{o}C for four passes; (3) 125 ^{o}C for two passes; and (4) 115 ^{o}C for two passes. All the ECAE passes were

followed by route A, using a 120^{o} angle die to attain minimum grain size in this alloy. The grains were refined to ~0.370 μm and the yield and ultimate tensile strengths of 372 MPa and 445 MPa were achieved, respectively along the ED (Figure 2.6). They suggested 180° rotation of the billet around ED between steps (1), (2) and (3), and 90° rotation between steps (3) and (4) results in successful completion of the whole extrusion procedure. But no mechanical responses were reported for this processing. Later Biswas et al. [67] were able to ECAE process pure Mg at room temperature using a similar temperature step-down technique starting from 250 °C. 8 ECAE passes were conducted following route A and leaded to an average grain size of ~250 nm. However, no information on the improvement of the mechanical properties was presented. They reported that they were not successful in processing the same procedure following routes B_C or C. They believe that this might be due to basal planes not orienting favorably along the shear plane of ECAE.

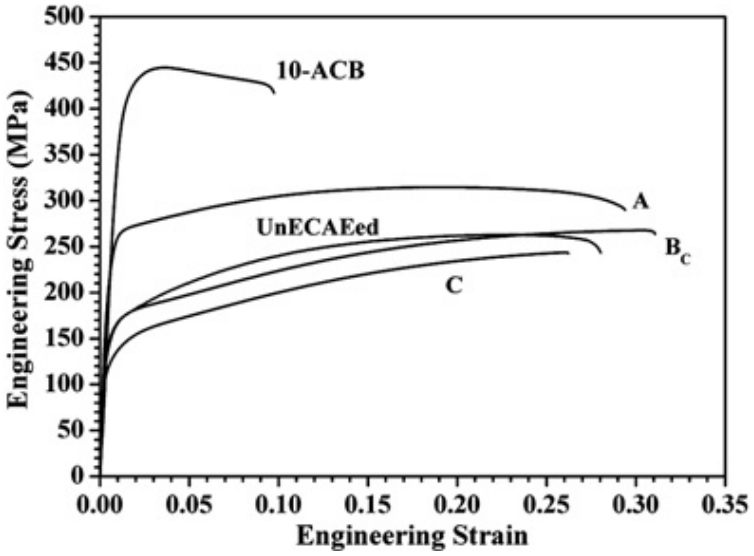

Figure 2.6 Mechanical response of ECAE processed billets by different processing routes for four passes and the multiple-temperature procedure [36].

Just recently, Foley et al. [73] processed AZ31B, following a five-step hybrid route and decreased the processing temperature from 200 °C down to 125 °C for the last pass. The procedure included two extrusion passes using route A (no rotation between passes, 2A) at 200 °C, a 180° rotation around the billet's long axis, another 2A at 150 °C, and another 180° rotation and one pass at 125 °C. They showed compressive strength levels in the processed sample, up to 350 MPa in yield and 500 MPa in ultimate strengths. But no tension test results were reported.

The initial texture significantly affects the evolution of texture, DRX, and grain morphology during ECAE due to different amounts of non-basal slip activity. The increase in Schmid factor for the basal slip and comparative reduction in Schmid factor for non-basal slip, results in more workability of the material [61, 67]. A work by Al-Maharbi et al. [72] investigated the effect of the initial texture on the microstructure and texture evolution of hot rolled AZ31B alloy during the first pass of ECAE. The billets were inserted to the ECAE die with their basal poles parallel to either the extrusion direction (ED) or the flow direction (FD). They observed that the former results in much lower flow stress anisotropy and tension/compression (T/C) asymmetry and more predominant DRX than the latter.

CHAPTER III

EXPERIMENTAL METHODS

3.1 Material

The research material was a type of Mg alloy called AZ31B (2.5-3.5 wt. % Al, 0.7-1.3 wt. % Zn, 0.2-1.0 wt. % Mg and balance-Mg) from a hot rolled plate. Magnesium and its alloys are the lightest of all structural metals. This Mg alloy was chosen because it represents the highest production wrought Mg alloy and also it has a relatively simple crystallographic texture [74].

3.2 Thermomechanical Processing of AZ31B Using Equal Channel Angular Extrusion

Billets with a cross-section of 25 mm × 25 mm and a length of 150 mm were machined from the hot rolled AZ31B. Mg alloys need to be processed at elevated temperatures to avoid fracturing [22]. However, during plastic deformation, basal plane would strain-harden, whereas prismatic and pyramidal planes would recover to get strain-softening, enabling us to run ECAE on this alloy at lower temperatures [67]. The first four passes were carried out at 200 °C [22]. Extrusion rate was kept at 0.075 mm/s for all the passes except for the passes at 125 °C, which was reduced to 0.038 mm/s to suppress shear localization [73, 75]. The furnace was heated to the desired temperature and both the billet and the die walls were lubricated. The billet was inserted to the die and held for 20 minutes for the first pass and 15 minutes before additional passes. After

each pass, the billet was water quenched. The back pressure was increased from 7 MPa to approximately 80 MPa by increasing the number of passes on a single billet. Since a lot of number of passes will be applied and after each pass the billet needs to be machined, care should be taken to preserve as much material as possible. Applying back pressure is necessary to increase the hydrostatic pressure and prevent cracking during processing. On the other hand, if we apply higher back pressure than actually needed, the billet will expand (fatten) and sometimes get stuck in the die. These ECAE parameters were found, after many trials, to be necessary to process the alloy without major shear localization or cracks due to the instability of deformation structure [76]. A die having a sharp 90° corner angle was used.

Four ECAE passes were conducted, to see the effects of ECAE routes on texture following the well-established conventional ECAE routes A, C, E and B_C. In route A, the billet is reinserted into the die without any rotation, but in routes C and B_C, the billet is rotated about its extrusion axis by 180° and 90°, respectively, before the consecutive pass. Route E is a combination of the routes C and B_C, where the billet is rotated around its extrusion axis by 180° before even-numbered passes and by 90° before odd-numbered passes. In addition, there is also unavoidable 90° rotation of the billet around its FD when it is inverted back to the vertical insertion orientation before the following pass. Details on the ECAE processing in general are presented in Chapter II. Billets need to be machined to the initial geometry before each pressing for multiple passes. More billets were ECAE processed at lower temperatures following the four passes at 200 °C to investigate the effect of grain size reduction on the activation of deformation

mechanisms and strength of the material. In the present work, the lowest deformation temperature is 100 °C and the maximum number of passes is 7.

All extrusions conducted on AZ31B alloy are listed in Table 3.1. The goal is to be able to run ECAE at lower temperatures without shear localization or cracking. Thus, texture plays an important role on making this deformation possible. Activating mainly basal slip because of its low CRSS is favored during simple shear of ECAE. The other experiments were continued mostly after cases 4A and 4C for this matter. These passes were carried out at lower temperatures which resemble A and C routes. The rationale behind these route selections was controlling the crystallographic texture to first suppress twinning during processing, which results in poor formability [75], and also aligning basal planes along the ECAE shear plane to orient them favorably [77]. This method increases the dislocation density fraction in the basal plane, making the CRSS ratio of the non-basal to basal planes less [67]. As a result, deformation of AZ31B at lower temperatures will be possible [67].

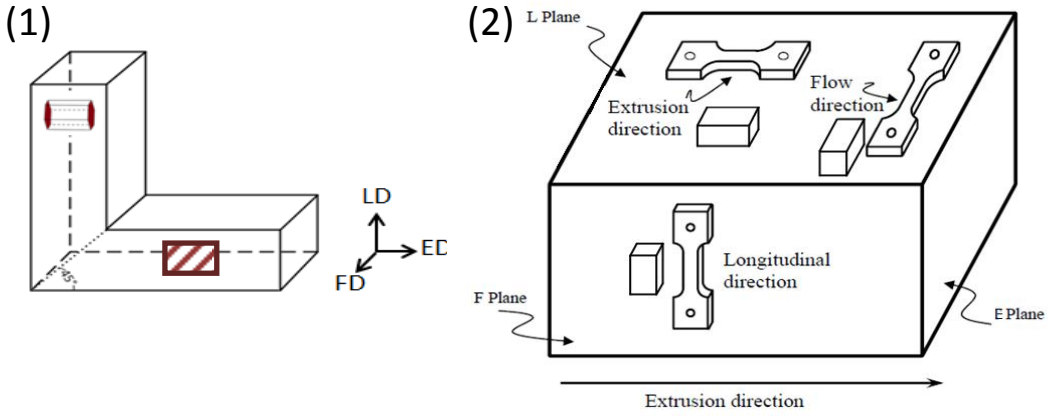

Figure 3.1 (1) Schematic showing the initial orientation of the basal planes in the billet and the three orthogonal directions, (2) Orientation of mechanical test samples on the as-processed billet.

3.3 Mechanical Testing of As-received and Processed AZ31B Alloy

Dog-bone shaped tensile specimens with nominal gauge dimensions of 8 mm × 3 mm × 1.5 mm and rectangular prism compression specimens with nominal dimensions of 4 mm × 4 mm × 8 mm were prepared using wire electrical discharge machining (EDM) from the fully deformed region of the extruded billets . The tension and compression tests were performed at room temperature using an MTS test frame along the three orthogonal directions of the ECAE billets: ED, FD and longitudinal direction (LD) as shown in Figure 3.1 (2). The experiments were conducted under strain rate control with a rate of 5×10^{-4} s^{-1}. At least three compression and tensile specimens were used to validate the repeatability of the experiments.

3.4 Microstructural Characterization of As-received and Processed AZ31B Alloy

Optical microscopy (OM), scanning electron microscopy (SEM), transmission electron microscopy (TEM), crystallographic texture measurements were performed on the samples cut from the fully deformed region of the billets with surfaces parallel to the flow plane which is perpendicular to FD as shown in the dashed region in Figure 3.1 (1) Texture measurements were carried out using X-ray diffraction with a Bruker AXS D8 Discover Diffractometer with Cu-Kα radiation at 40 kV and 40 mA. For optical microscopy and SEM, the samples were mechanically polished down to 0.04 μm and etched using a solution that is composed of 5 mL acetic acid, 3 g picric acid, 10 ml H_2O and 90 ml ethanol. The optical micrographs were taken using a Keyence VHX-600K digital microscope. For higher resolutions a Keyence VH-Z500 was used. SEM images

were taken using a JEOL JSM-7500F ultra high resolution field emission scanning electron microscope (FE-SEM).

For TEM, the specimen was cut in 3 mm diameter disc parallel to FP and ground to a thickness of less than 80 μm. Specimens were ion polished at 4kV, 3 kV and finally at 2 kV, with Gatan 691 Precision Ion Polishing System (PIPS). The foils were examined with a JEOL JEM 2100 TEM with a LaB_6 filament operated at 200 kV.

Table 3.1 A list of ECAE experiments carried out on AZ31B Mg alloy.

	Route	pass	Temperature		Route	pass	Temperature		Route	pass	Temperature		Route	pass	Temperature
1	A	4	200	+				+				+			
2					A	1	150								
3					C	1	150								
4					C	1	150		C	1	125				
5					C	1	150		C	1	125		A	1	125
6	C	4	200												
7					C	1	150								
8					C	1	150		C	1	100				
9					C	1	150		C	1	125				
10					A	1	150								
11	E	4	200												
12					C	1	150								
13	B_C	4	200												

CHAPTER IV

RESULTS AND DISCUSSIONS

As a basis of comparison, the microstructure and mechanical response of the as-received (AR) material were first determined. Figure 4.1 shows three orthogonal directions of the hot rolled plate: rolling direction (RD), transverse direction (TD) and normal direction (ND). The grains in the hot rolled AZ31B plate were equiaxed and had an average size of 25 μm. As expected a strong basal texture in which basal poles are parallel to ND was measured (Figure 4.2).

Figure 4.2 (4) shows the true tensile and compressive stress-strain responses of the AR plate at room temperature. The specimens yielded at 158 and 58 MPa in tension along the RD and ND, respectively. In compression however, the specimens yielded earlier along RD with a 0.2% proof stress value of 69 MPa compared to 182 MPa along ND. This clearly shows the anisotropic behavior of this material. Due to the same orientation most of the grains have, relative to the applied load along both RD and TD, the mechanical responses are almost similar. Thus only the mechanical responses along RD are presented here. However a work by Jain et al. [47] shows that because the angular spread in the pole density is greater towards RD than towards TD, there is a higher degree of twinning for RD tension than for TD tension [47].

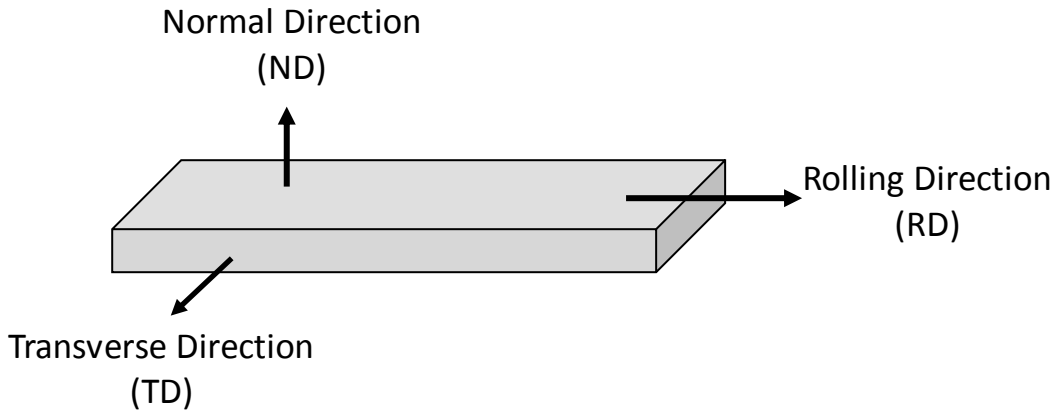

Figure 4.1 Three orthogonal directions of the hot rolled AZ31 magnesium alloy.

The effect of applying one pass of ECAE on AZ31B has been thoroughly investigated previously [59, 61, 78]. The purpose of this research is to process the AZ31B Mg alloy using ECAE following certain processing routes, temperatures and different numbers of ECAE passes.

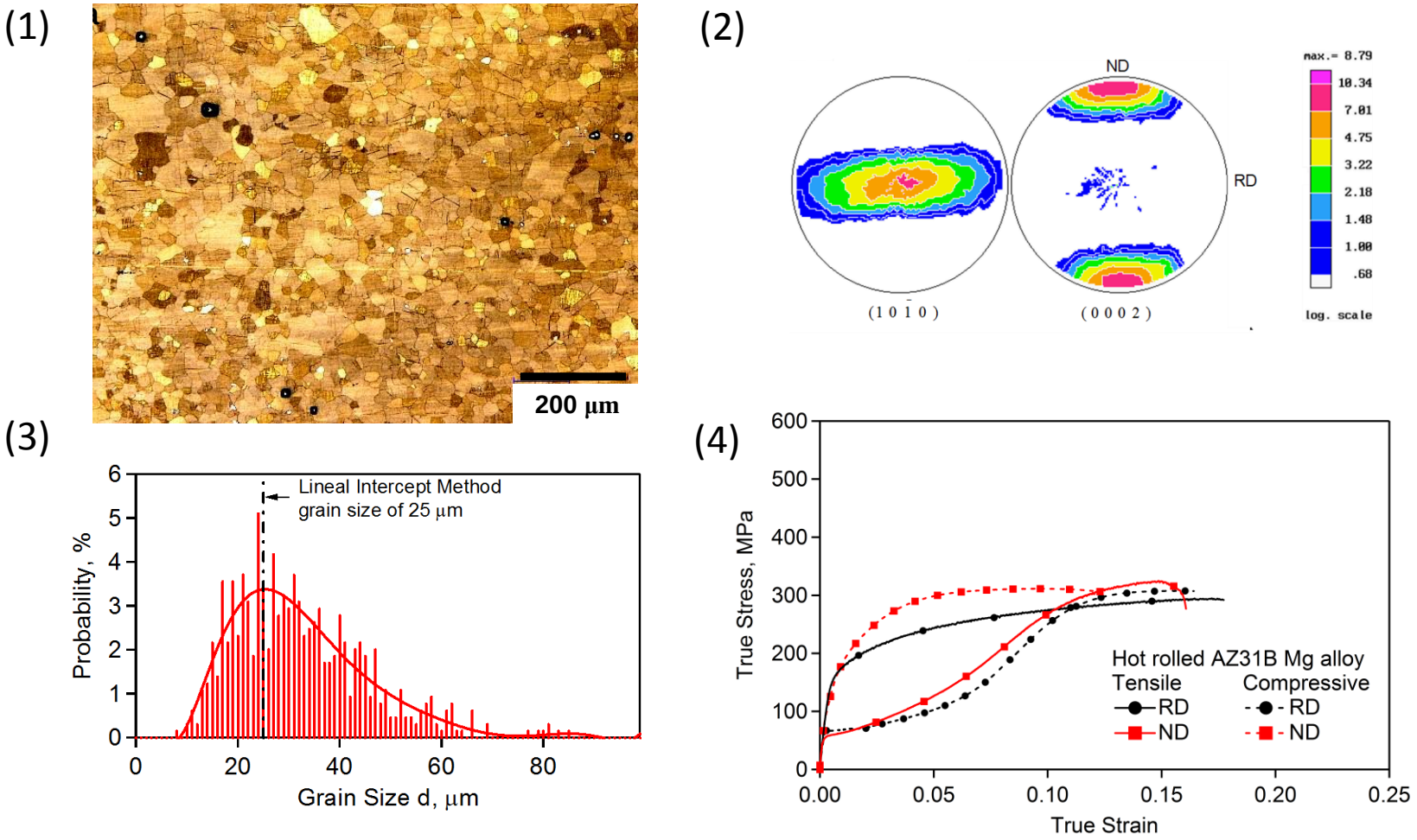

Figure 4.2 (1) The microstructure, (2) texture, (3) grain size distribution, and (4) room temperature tensile (solid lines) and compressive (dashed lines) responses along the two plate directions: rolling direction (RD) and normal direction (ND) of as-received (AR), hot rolled AZ31B alloy [61].

4.1 The Effect of ECAE Route on High Temperature Processed Samples

In this study, four billets were ECAE processed following routes A, C, E and B_C up to four passes, referred to as 4A, 4C, 4E and $4B_C$. The starting texture of all of them was the same, having basal poles parallel to ED (Figure 3.1 (1)). With selecting this initial texture, DRX was more dominant in the first ECAE pass, which resulted in better refinement of grains [72]. Four different routes were chosen to investigate the texture evolution during ECAE and its effect on mechanical properties and microstructure. Optical micrographs of these cases shown in Figure 4.3, depict the grain size and microstructural morphology of these samples. The grain size was calculated by measuring the size of about 300 – 400 grains. Route B_C produced the most uniform microstructure with the smallest grain size of about 2.7 μm, which is in agreement with literature (e.g. [34, 60]). Samples processed following routes A and C have close grain sizes of ~4 μm but the 4C sample is slightly more inhomogeneous. SEM was also carried out to check the validity of the grain sizes measured by OM images. Figure 4.3 (5) shows SEM image of 4A, which was selected for this comparison. By using the same previous method of measuring the size of a large number of grains, a smaller average grain size of ~2.8 μm was obtained. The reason for this variation between the two results can be supported by the fact that SEM is a more accurate technique for measuring grains as small as nano-scale size. Figure 4.4 shows the broad grain size distribution of 4A, measured using both OM and SEM images.

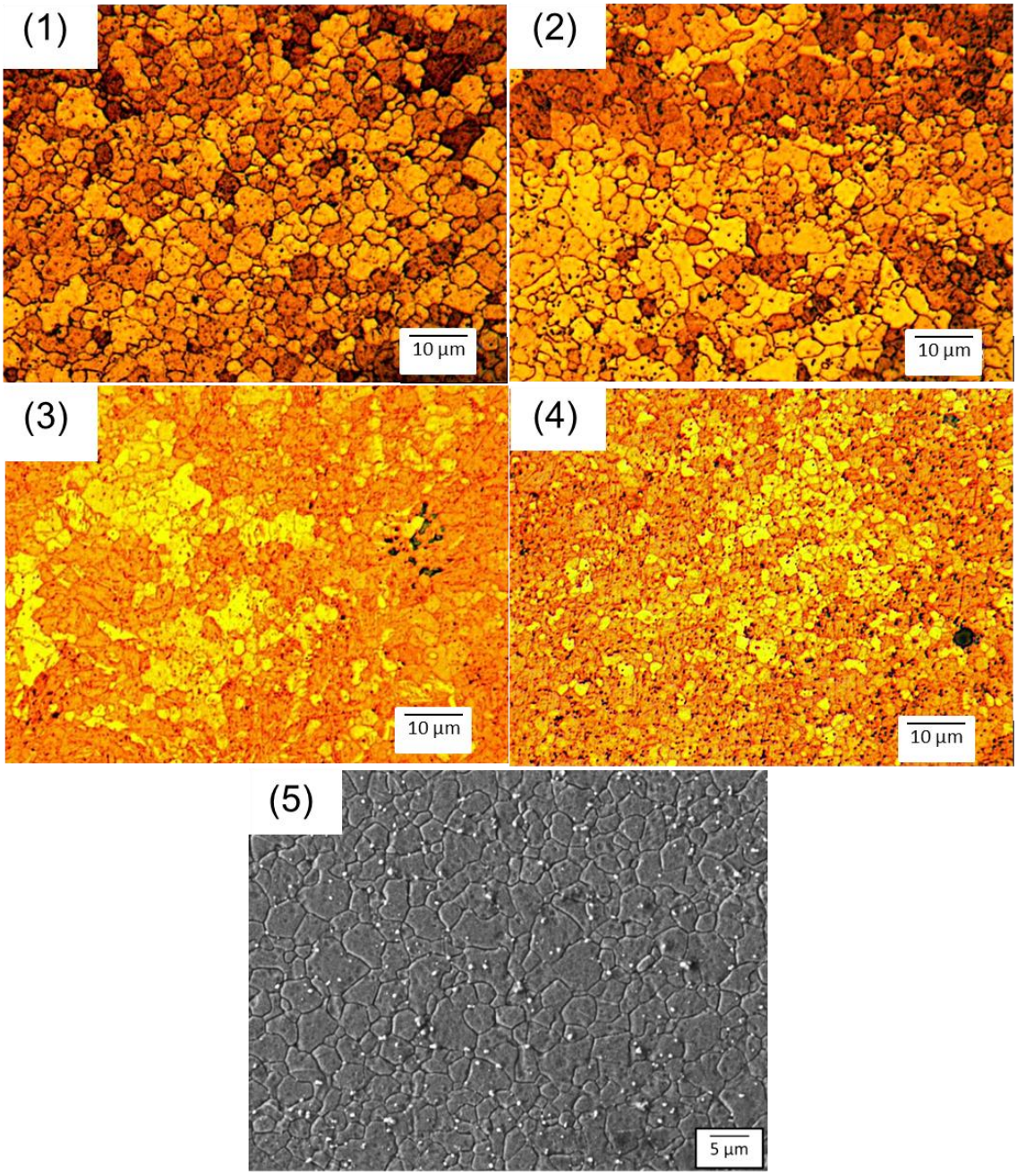

Figure 4.3 Optical micrograph images of AZ31B ECAE samples processed up to four ECAE passes and following routes (1) A, (2) C, (3) E, (4) B_C [61, 77] and (5) Secondary electron image of 4A showing equiaxed grain structure.

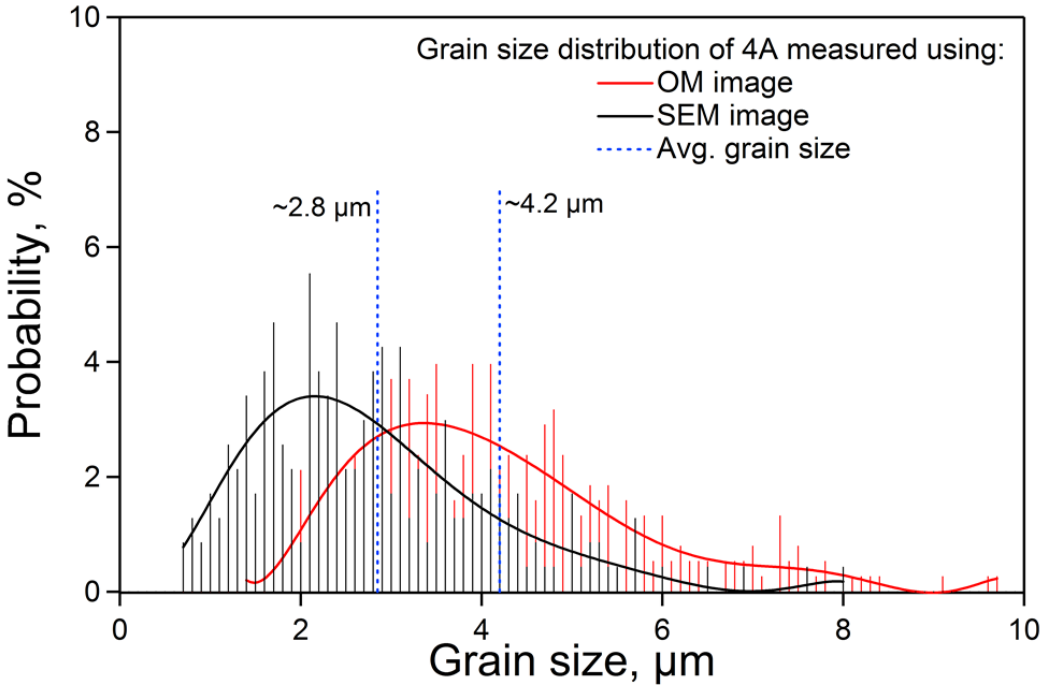

Figure 4.4 Grain size distribution of AZ31B sample processed up to four ECAE passes following route A calculated using optical and secondary electron micrographs..

In general, we can argue that after four passes of ECAE the sample shows a reasonably homogenous structure in the AZ31B alloy regardless of the route chosen, which is different than aluminum alloys processed by ECAE [79]. The grain size of ~25 µm in the AR AZ31B was decreased to ~3µm on the average after four ECAE passes. This refinement is because of the continuous shearing of the grains and DRX occurring during the ECAE process.

Figure 4.5 shows the basal and prismatic pole figures of the 4A, 4C, 4E and $4B_C$ samples from the flow plane of the billet. In 4A and 4C, two basal peaks sit around the rim of the stereographic projection, which are closer in case 4A and apart from each

other in 4C. In $4B_C$ and 4E the texture is more spread, but still most of the grains are oriented perpendicular to FD. This is the result of the 90° rotation around ED in these two routes.

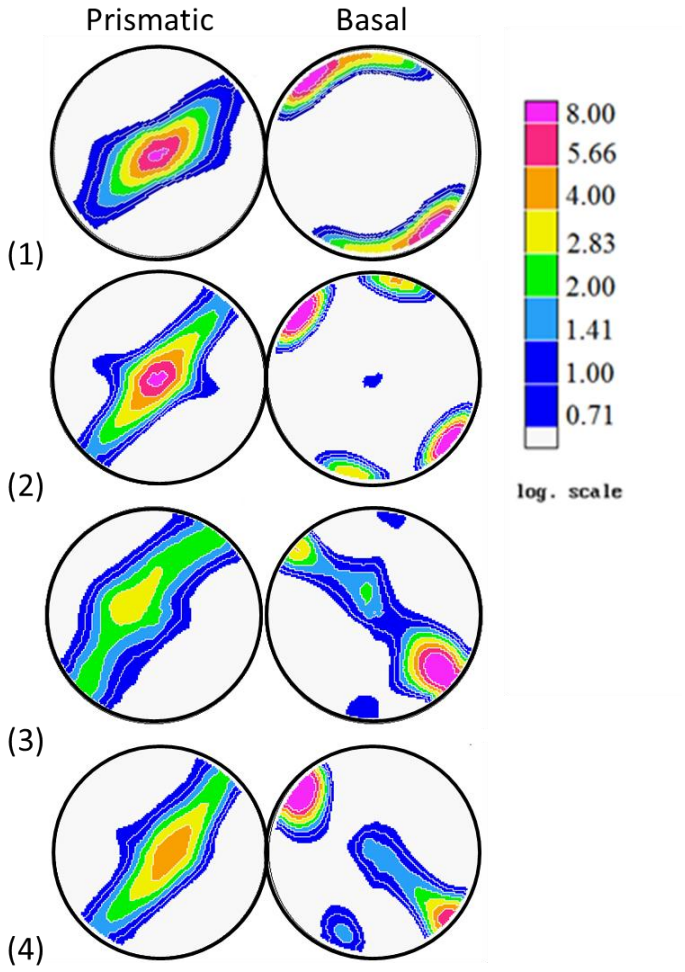

Figure 4.5 Basal and prismatic pole figures of (1) 4A, (2) 4C, (3) $4B_C$ and (4) 4E.

The mechanical responses of the samples that went under four passes of ECAE are shown in Figure 4.6. Tensile loading parallel to the c-axis (basal poles) of the most Mg alloys are expected to result in tensile twinning [75, 80]. This can be easily seen in

the experimental data. A plateau region with a relatively steady stress level [75] or a low hardening coefficient followed by an upward curvature with a high hardening rate is an indication of twinning activation in hcp materials [77]. For instance, compression along FD in both the 4A and 4C cases shows this phenomenon. The activation of tensile twinning attempts to lower the yield strength [72]. For instance, 4C yielded at ~240 MPa in FD tension and ~143 MPa in FD compression. In the other two cases, there is a good amount of grains oriented differently so we expect some slip systems other than twinning to be activated. However, all of these samples yield almost at the same stress value of about 150 MPa under compression along FD.

The mechanical responses of the 4E and $4B_C$ samples are very close to each other due to their similar textures they generate during processing shown in Figure 4.5. We can clearly see that the more the texture is spread, the less flow stress anisotropy and T/C asymmetry are observed. Since twinning is unidirectional and it only activates in a certain direction, it leads to the T/C asymmetry. For instance, 4A and 4C show a strong basal texture and flow stress anisotropy is more pronounced in these two cases, respectively [77].

A big change was seen in mechanical responses along different directions due to the operation of different deformation mechanisms. To show this fact, tension along FD in cases 4A and 4C demonstrated a typical downward hardening associated with slip dominated deformation. Basal poles were almost perpendicular to FD in these two cases (Figure 4.5). Based on the previous reports, when the c-axis is constrained, prismatic slip is expected to be favorable when twinning is not a possibility [47, 81, 82]. In all the four

cases, samples showed the highest strength when pulled along FD. Interestingly, T/C asymmetry was more pronounced along this direction.

If the angle between the applied stress and the basal peak is around 45°, basal slip is favored. Since basal slip is the easiest deformation mechanism in Mg alloys to be activated, the sample tends to yield at very low stress levels. In all the cases, this is true when the sample was in tension or compression along ED, since there is a pronounced basal peak oriented 45° from ED. But as can be seen in Figure 4.5, there is a slight difference in case 4A. The samples showed twinning behavior in ED when compressed. That is due to the difference in the texture of 4A from the other textures, having some grains oriented in a way that their basal poles are aligned to LD. Thus, when the sample is compressed along ED or pulled along LD, those grains twin.

For better comparing the results, Table 4.1 lists yield and ultimate strengths for all the four billets processed at 200 °C followed by different routes, along the three orthogonal directions.

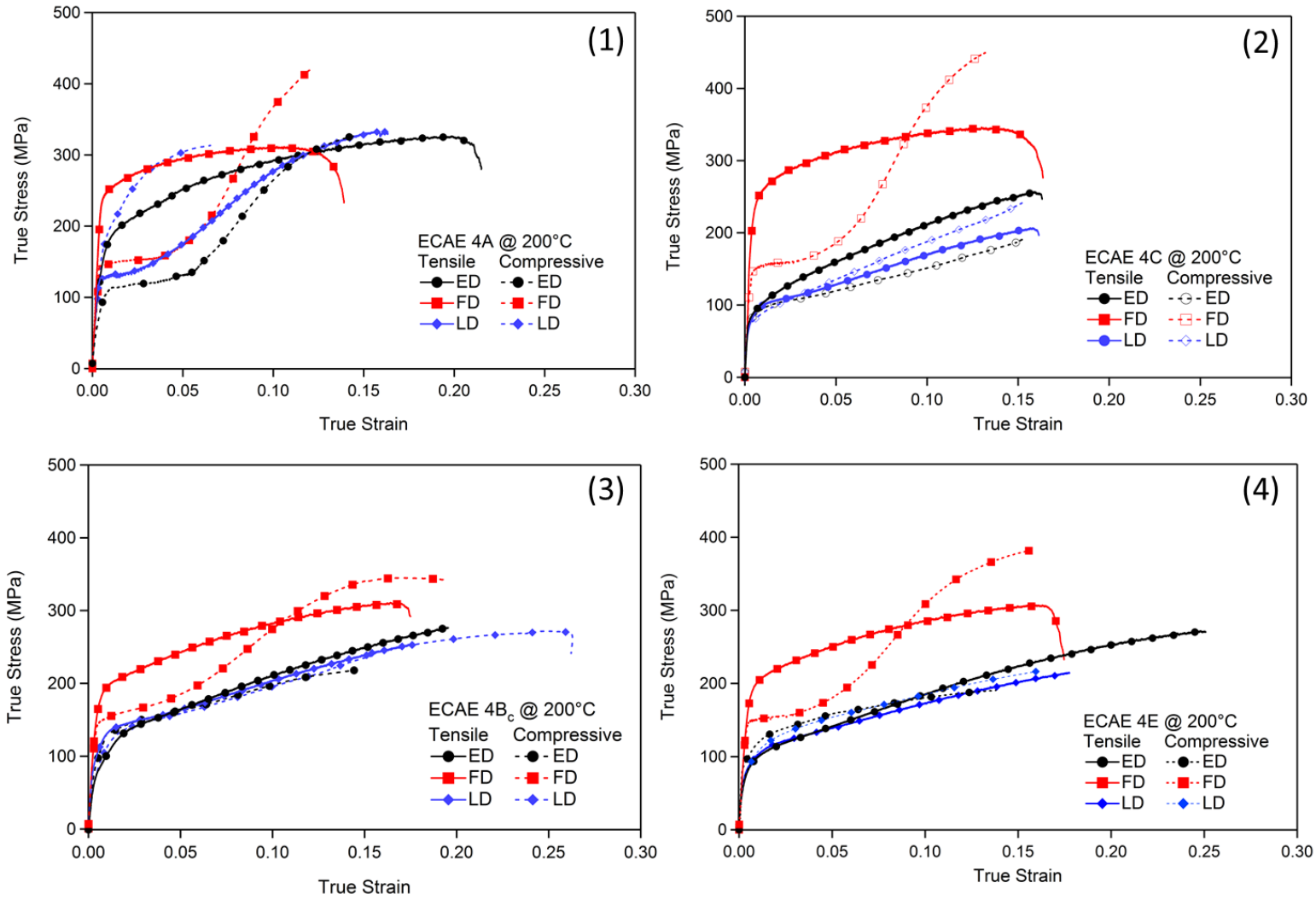

Figure 4.6 Room temperature tensile (solid lines) and compressive (dashed lines) true response of AZ31B alloy ECAE processed up to four passes following route (1) A, (2) C, (3) E and (4) B_C.

Table 4.1 Mechanical properties of ECAE processed AZ31B Mg alloy under tension and compression. The number before the billet label indicates the number of passes, and the letter represents the ECAE route. (ED: Extrusion Direction, LD: Longitudinal Direction, FD: Flow Direction).

Billet	Direction	Tension		Compression	
		0.2% proof stress (MPa)	UTS (MPa)	0.2% proof stress (MPa)	UTS (MPa)
4A	ED	146.35 ±16.47	328.55 ±2.61	114.25 ±8.84	332.85 ±8.84
	LD	127.1 ±1.20	306.8 ±38.32	182.75 ±6	310.4 ±4.24
	FD	243.8 ±0.42	314 ±3.32	149.25 ±6.29	419.5 ±0.7
$4B_C$	ED	83.91 ±3.0	262.9 ±13.6	100 ±1.41	211.6 ±10.18
	LD	98.5 ±0.15	249.3 ±5.7	99.25 ±11.75	276 ±4.0
	FD	170.7 ±2.3	308.11 ±4.08	140 ±7.07	341.15 ±5.3
4C	ED	78.86 ±8.85	251.4 ±7.7	78.75 ±2.33	189.2 ±5.37
	LD	78.1 ±1.69	189 ±25	62.4 ±17.11	221.3 ±29.56
	FD	239.3 ±14.84	312.7 ±33.4	143.1 ±7.85	441.7 ±8.3
4E	ED	74.75 ±8.25	268 ±5.73	86.6 ±8.56	186.2 ±6.27
	LD	81.59 ±3.69	213.78 ±1.69	85.05 ±0.18	216.6 ±6.78
	FD	183.5 ±6.77	303.6 ±5	143.79 ±6.78	365.8 ±23.33

4.1.1 Summary of observations

AZ31B Mg alloy was successfully processed up to four passes following routes A, C, E and B_C. The mechanical responses of the processed samples revealed the significance of the crystallographic texture on the flow stress anisotropy and T/C asymmetry. The main findings of this study can be summarized as follows:

1. Routes E and B_C result in more uniform microstructures than those produced by routes A and C. Route B_C leads to the finest grain size.
2. The activity of tensile twinning during monotonic testing leads to the T/C asymmetry.

4.2 The Effect of the Billet Rotation between ECAE Passes on Low Temperature Processability and Mechanical Response

The AZ31B Mg alloy was processed using thermo-mechanical hybrid routes that include ECAE at different temperatures. 200 °C ECAE processing of AZ31B Mg alloy triggers dynamic recovery and recrystallization, so it contradicts our ultimate goal, which is strengthening the material by refining its grain size. Therefore, low temperature processing after the initial high temperature processing is necessary to prevent dynamic recovery and recrystallization. In this work, ECAE processing at lower temperatures were systematically studied. We lowered the processing temperature incrementally from 200 °C to 150 °C during ECAE passes. According to Table 3.1, all the additional passes were either applied without any rotation or with a 180° rotation around ED. The effect of

this rotation between the ECAE passes on low temperature processing and mechanical properties of the as-processed samples were investigated.

4.2.1 The effect of a 180° rotation of the billet between low temperature ECAE passes

First, we focus on the cases that a 180° rotation was applied for the low temperature ECAE passes. As explained in section 3.2, for the first step, which is conducting four ECAE passes at 200 °C, mostly 4A and 4C were chosen. These two cases have relatively easy-to-deform textures for low temperature ECAE processing when inserted into the die by a 180° rotation. By this rotation most of the basal planes will orient along the shear plane. There are notable grains oriented differently in 4E and $4B_C$, activating non-basal slips during ECAE. However, a hybrid route starting with 4E (case #12 in Table 3.1) was selected to see and analyze its effect on texture and grain morphology during the fifth pass of ECAE. For the second step of multi-temperature ECAE processing, the processing temperature decreased to 150 °C to begin sub-micron grain levels in the alloy.

An additional pass at 150 °C with a 180° rotation around ED (which we refer to as 1C, since it resembles route C) was applied after 4A, 4C and 4E. The extrusion rate was kept at 0.075 mm/s and back pressure was increased to 48 MPa to avoid cracking for all the three cases. These cases will be referred to as 4A+1C, 4C+1C and 4E+1C. The numbers in this labeling indicate the number of ECAE passes that were applied at certain processing temperatures and the letters represent the type of the routes chosen. These

letters do not follow a standard labeling, but they are only used to illustrate the processing conditions more easily.

Optical images of 4A+1C, 4C+1C and 4E+1C are shown in Figure 4.7. It is apparent that 4C+1C and 4E+1C have the most and the least uniform grain size distributions, respectively. In 4E+1C, there are elongated grains all through the sample with their long axis parallel to shear band (SB) orientation [83].

In order to better visualize the grain size and morphology, SEM was carried out on 4A+1C. According to Figure 4.7 (4), the grain morphology seems to be homogenized and the average grain size measured was ~0.6 μm.

The measured basal and prismatic pole figures are shown in Figure 4.8. 4C+1C and 4E+1C have similar textures. They both have a strong basal peak oriented 45° (CCW) from LD but there are some differences between their second basal peaks. The reason could be the difference between the pre-processed textures. In 4A+1C, in addition to that ~45° basal peak, there is a strong peak oriented parallel to LD.

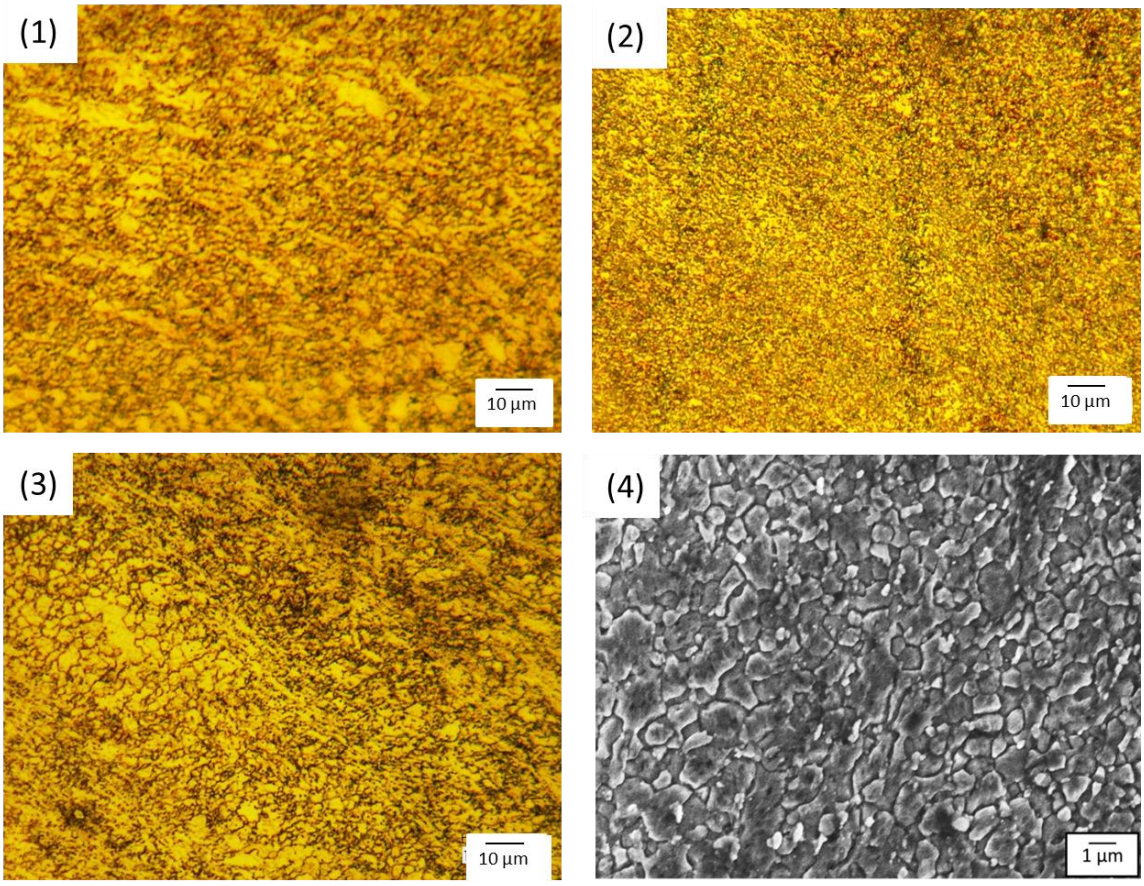

Figure 4.7 Optical micrographs of AZ31B ECAE samples processed by (1) 4A+1C, (2) 4C+1C, (3) 4E+1C and (4) Secondary electron image, showing a fine-grained structure of 4A+1C.

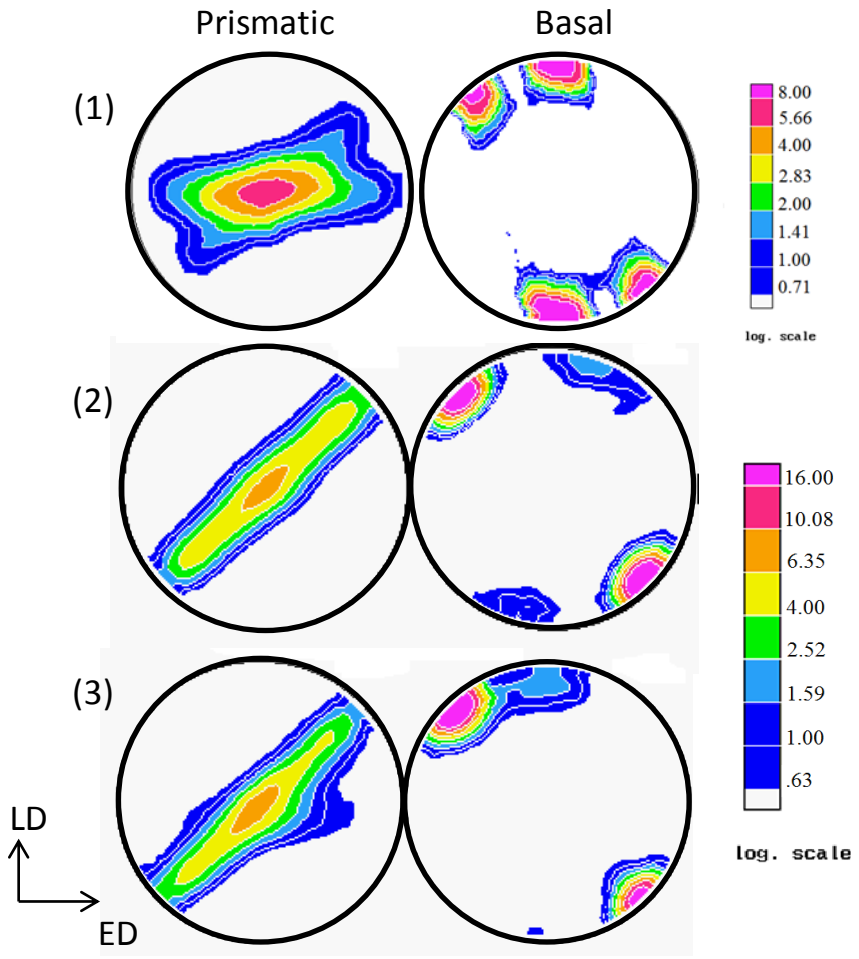

Figure 4.8 Basal and prismatic pole figures of (1) 4A+1C, (2) 4C+1C and (3) 4E+1C.

Tension and compression tests were conducted along the three orthogonal directions for all the cases at room temperature. The results are presented in Figure 4.9. Since 4C+1C and 4E+1C have similar orientation of basal poles with respect to both ED and LD, there is little difference between the ED and LD responses whether in tension or compression. These two samples are very ductile in the aforementioned directions,

because of the activation of mainly basal slip. Moreover, because the textures have been strengthened for the fifth pass; flow stress anisotropy was enhanced in both.

A large amount of grains in the 4A+1C sample have basal poles aligned with LD and almost perpendicular to ED and FD. Thus, tension along LD or compression along ED place most of the grains in c-axis tension, which is accommodated mostly by tensile twinning [84].

Table 4.2 lists the 0.2% proof stresses and ultimate strengths of all the samples tested. In tension, all the samples exhibited higher tensile yield strength and subsequently lower work hardening at the later stage of deformation when tested along FD than those tested along LD and ED. Such directional dependence can be associated with the activation of different deformation mechanisms. Due to the directionality of twinning, the compressive load along FD produces the opposite response than what was observed in tension.

The 4A+1C sample broke at 5% of strain along LD compression. In some previous works, a compressive twinning was reported in Mg alloys when a stress is applied parallel to the c-axis. The activation of this mechanism tends to make the material very brittle at room temperature, since compressive twinning systems are very temperature-dependent [75, 85-87]. The basal peak aligned with LD could be responsible for this low ductility, but on the other hand, it also resulted in a high yield strength.

Overall, 4A+1C showed higher yield and ultimate strengths compared to the other two, due to having the second intense peak oriented along LD.

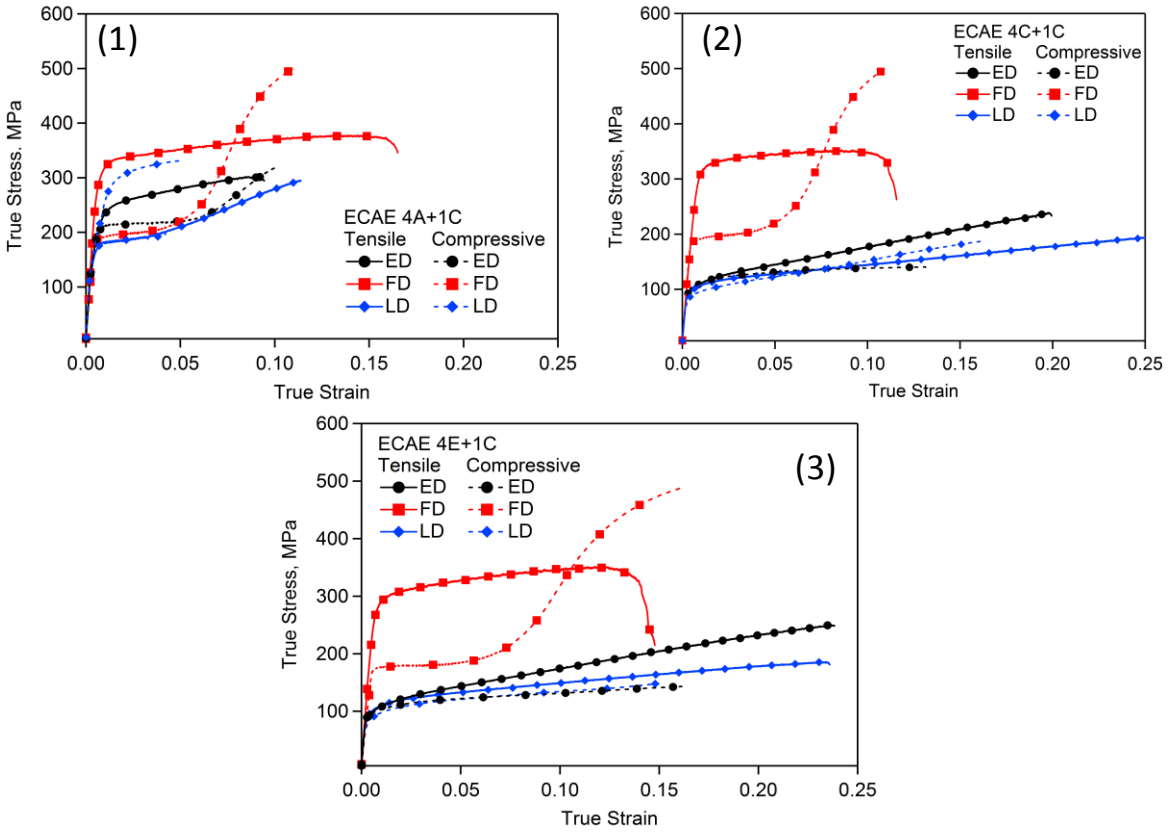

Figure 4.9 Room temperature mechanical responses of the AZ31B Mg samples processed via (1) 4A+1C and (2) 4C+1C and (3) 4E+1C.

There are many parameters that need to be accounted for designing the routes, including activating basal slip during ECAE processing, uniformity of grains and avoiding shear localization. So, 4E+1C seemed to not be a good choice for further processing at lower temperatures because of not having a uniform grain structure. On the other hand, 4A+1C and 4C+1C satisfied the aforementioned requirements.

Table 4.2 Tension and compression response of AZ31B Mg alloy ECAE processed using temperature strep-down method following routes 4A+1C, 4C+1C and 4E+1C.

Billet	Direction	Tension		Compression	
		0.2% proof stress (MPa)	UTS (MPa)	0.2% proof stress (MPa)	UTS (MPa)
4C+1C	ED	94.7 ±2.48	229.34 ±13.79	100.52 ±2.72	141.5 ±1.15
	LD	95.54 ±0.52	198.06 ±4.49	86.72 ±0.88	182.41 ±6.95
	FD	306.21 ±6.36	346.89 ±7.15	180.41 ±10.68	497.71 ±2
4E+1C	ED	96.49 ±0.08	246.94 ±4.03	92.1 ±4.10	143.82 ±0.76
	LD	97.6 ±0.73	180.53 ±7.45	90.53 ±3.63	168.52 ±28.5
	FD	281.3 ±3.25	354.25 ±4.45	167.33 ±9.6	477.13 ±14.06
4A+1C	ED	222.8 ±8.06	294.5 ±10.04	194.6 ±14.92	287.4 ±42.9
	LD	172 ±2.33	289.3 ±8.27	273.8 ±20	328.2 ±4.16
	FD	303.6 ±6.36	372.1 ±8	261.9 ±6.73	521.4 ±1.97

4.2.2 The effect of no billet rotation between the low temperature ECAE passes

In this section, we focus on processing the AZ31B billet at a lower temperature but without any rotation between the passes (resembling route A). Having mentioned the reason in section 4.2.1, we continue low temperature processing on cases 4A and 4C. An

ECAE pass was performed at a temperature of 150 °C without any rotation followed by 4A and 4C at 200 °C. The processing conditions were the same as the previous cases explained in section 4.2.1. These two processing cases will be designated 4A+1A and 4C+1A, accordingly. Their optical micrographs are shown in Figure 4.10. 4A+1A showed a nearly homogenized microstructure. The grain size was reduced to less than 1 μm. In 4C+1A, there are some relatively larger grains surrounded by smaller grains.

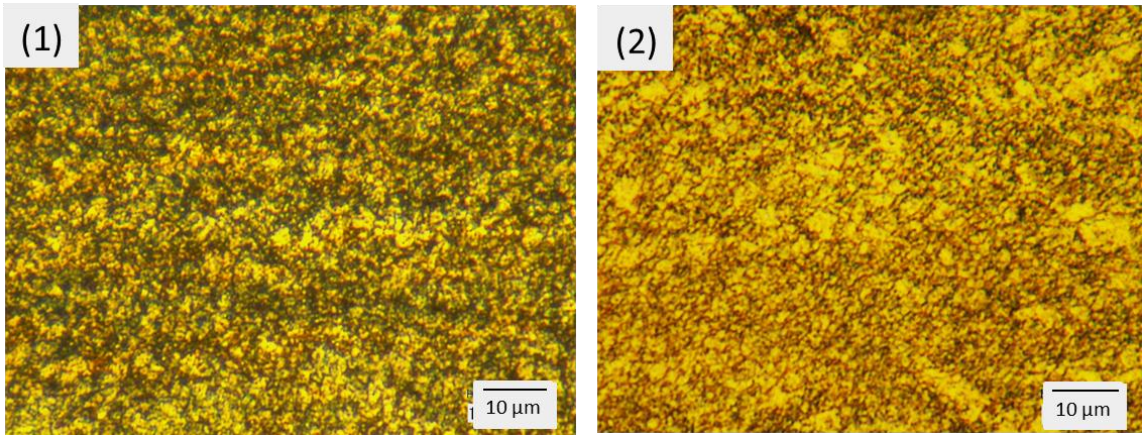

Figure 4.10 Optical micrographs of AZ31B ECAE samples processed by (1) 4A+1A, (2) 4C+1A.

The measured basal and prismatic pole figures are shown in Figure 4.11. A single basal peak was formed almost parallel to LD in 4A+1A. This texture is almost similar to the AR texture. 4C+1A has a wide single peak spanning from 0° to 45° (CCW) from LD.

The responses of the two ECAE samples, 4A+1A and 4C+1A, in tension and compression are shown in Figure 4.12. The first observation from these curves is the low ductility seen in LD compression. Compression along LD, especially in the 4A+1A sample, was expected to mainly activate compressive twinning, and thus the samples

broke at low strain levels. But in the 4C+1A sample, this could be also the consequence of SBs in the sample; as there are some grains oriented favorably for basal slip and compressive twinning is possibly not the only active system. Moreover, low ductility was also observed in LD tension, which was not expected. Table 4.3 shows the average yield and ultimate strengths in tension and compression for both processed billets. Similar to all the previous cases in section 4.2.1, the trend in the flow stress anisotropy and T/C asymmetry can be correlated with the texture that develops after five-pass ECAE.

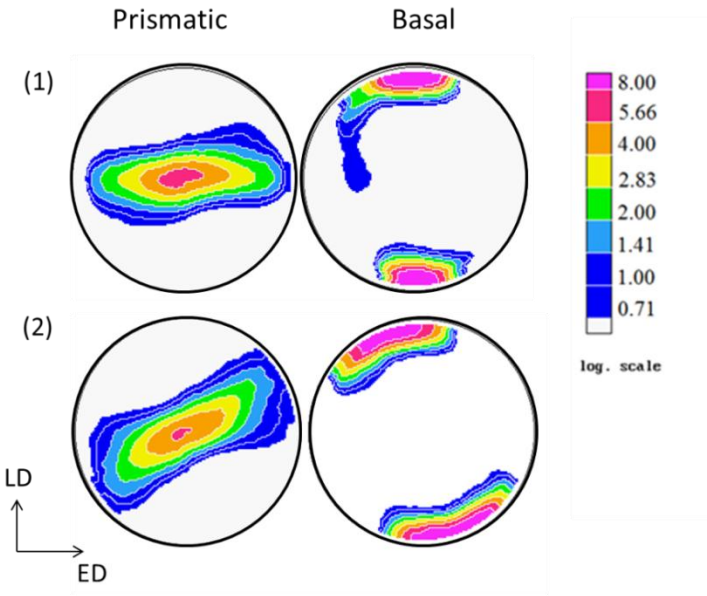

Figure 4.11 Basal and prismatic pole figures of (1) 4A+1A and (2) 4C+1A.

In 4A+1A, FD tension is likely accommodated by prismatic slip and FD and ED compression mainly by tensile twinning. The same trend is seen in 4C+1A, but with the exception that ED compression shows only a little tensile twinning behavior. Having a major number of grains oriented favorably for basal slip, this case behaved differently

along ED compression. Having compared the two cases, 4A+1A showed higher yield and ultimate strengths in all directions except FD tension. This can be supported by the fact that the basal peak in 4A+1A is more broadened to the FD. Thus, for those grains that are not exactly oriented perpendicular to the load, basal slip might activate.

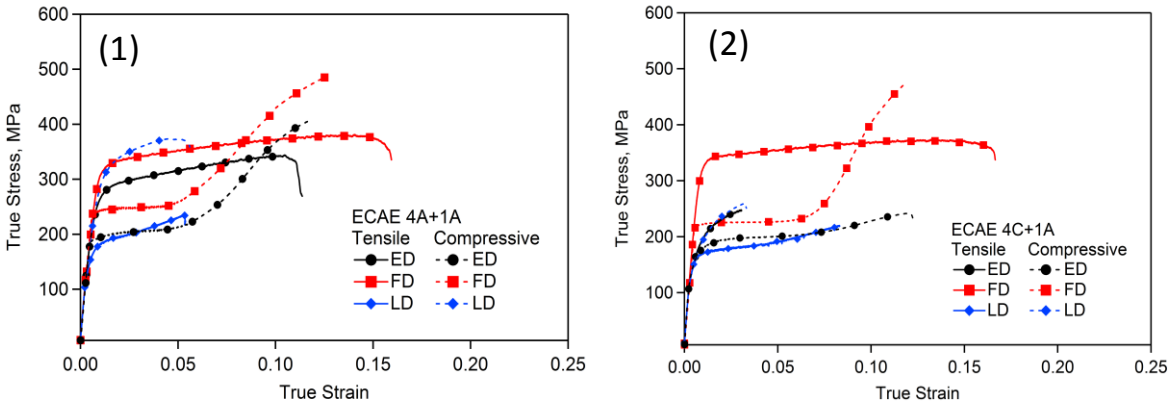

Figure 4.12 Room temperature mechanical responses of the AZ31B Mg samples processed via the hybrid route (1) 4A+1A and (2) 4C+1A.

Table 4.3 Tension and compression response of AZ31B Mg alloy ECAE processed using temperature strep-down method following routes 4A+1A, 4C+1A.

Billet	Direction	Tension		Compression	
		0.2% proof stress (MPa)	UTS (MPa)	0.2% proof stress (MPa)	UTS (MPa)
4A+1A	ED	260.9 ±0.58	346.49 ±3.43	185.94 ±6.33	408.46 ±0.28
	LD	162.34 ±6.13	243.5 ±12	275.69 ±6.7	369.65 ±5.23
	FD	304.75 ±4.84	373.39 ±5.6	235.54 ±2.9	478.5 ±5.49
4C+1A	ED	160.3 ±0.52	242.39 ±7.65	155.45 ±0.68	252.51 ±15.16
	LD	155.13 ±1.23	223 ±4.23	159 ±1.24	260.8 ±1.99
	FD	325.45 ±4.11	374.4 ±0.99	220.93 ±0.9	492.17 ±22.8

4.2.3 Summary of observations

From observing Figures 4.5, 4.8 and 4.11 showing the textures of all the processed billets so far, we can classify these textures into four categories of *A*, *C*, *A+C* and B_C textures. “A” texture (as was seen in AR texture) has a single spread peak parallel to LD, like in 4A+1A. Texture “C” has two peaks separated by 60-65° and they make an angle of about 45° from ED and LD. The basal peak that is located 45° from LD (CCW) is more intense. This group includes 4C, 4C+1C and 4E+1C. Texture “A+C”

has two peaks close to each other, one almost parallel to LD and the other close to 45° from LD, seen in 4A, 4A+1C. Or it can be a single peak spanning from 0° to 45° (CCW) from LD as in 4C+1A. At last in texture "B_C" basal poles are aligned along a pole making an angle of about 27-38° from LD, seen in 4E and $4B_C$. The mechanical responses in tension and compression of the samples in each category follow the same trend, meaning that similar deformation mechanisms were activated.

The AZ31B Mg alloy was successfully processed at 150 °C. This low temperature processing was conducted after 4A, 4C and 4E. The mechanical responses of the processed samples revealed the significance of the crystallographic texture. The main findings of this study can be summarized as follows:

1. Low temperature processing of the AZ31B Mg alloy was successful after initial high temperature processing. Smaller grain sizes were achieved using the temperature step-down method.
2. For the same group of textures, as we lowered the processing temperature, smaller grains were produced in the samples, resulting in more strengthening of the alloy.
3. Having type "A" texture gives higher strengths, on the other hand, "C" texture improves the ductility. "A+C" texture satisfies both needs, if processed successfully.

4.3 The Effect of Texture on Ultrafine-Grained AZ31B Alloy

In order to obtain a UFG AZ31B alloy, we lowered the ECAE temperature to 100 °C for the sixth pass to further saturate the dislocation density and to see if this incremental 50 °C decrease in processing temperature is feasible or not. For being able to run ECAE on AZ31B at low temperatures, we needed to induce a high amount of dislocation density on the basal planes to reduce the large difference between CRSSes of basal and non-basal slips. But, we needed to investigate if running only two passes at low temperatures and decreasing the temperature down to 100 °C would satisfy this claim. Thus, we chose 4C+1C and applied an additional pass at 100 °C followed by a 180° rotation around ED. For this pass, the billet was encapsulated in an interstitial-free (IF) steel can. This encapsulation was to enhance the hydrostatic force to suppress shear localization and cracking due to the difficulty of processing AZ31B at lower temperatures [73, 88]. The disadvantage of this technique is that the billet needs to be machined to fit into the IF steel can. Thus, we were unable to cut tensile samples along FD and LD. We refer to this case as 4C+1C+1C@100 °C (The reason for including the last pass's temperature in the labeling was that a similar case will be presented later, and we needed to somehow distinguish these two cases from each other).

The optical micrograph in Figure 4.13 shows SBs that are typical for shear localization and contain submicron grains [88] and obviously are not desired due to creating non-uniform grain size distribution.

The basal and prismatic pole figures of 4C+1C+1C@100 °C are shown in Figure 4.14 (1). Since only C routes were applied to the billet, the resulting texture falls in the

same category as “C” texture. The stresses applied from the IF steel can during ECAE are thought to be the reason for some grains orienting differently than predicted and also causing the SBs.

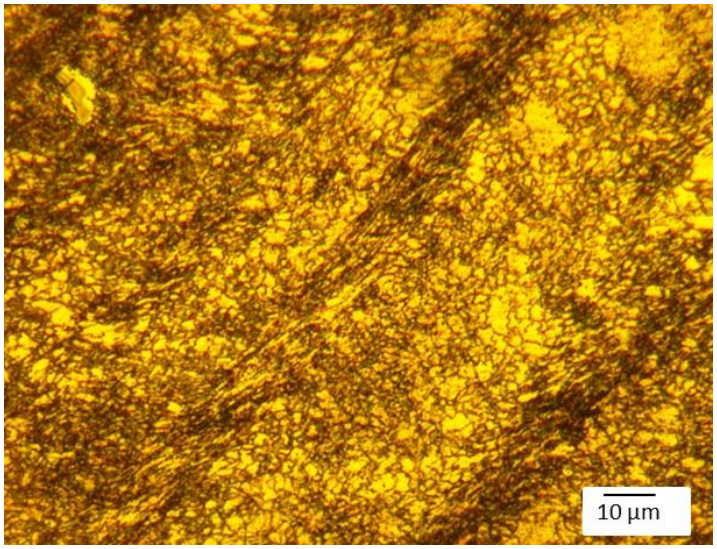

Figure 4.13 Optical micrograph of AZ31B ECAE samples processed by 4C+1C+1C@100 °C.

The compression stress-strain response along three orthogonal directions and also its tensile response along ED are presented in Figure 4.14 (2). The intense basal peak oriented ~45° away from ED must favor basal slip in ED tension, resulting in high ductility. However, the billet broke at very early stages when pulled along ED. This rapid fracture could be the result of the existence of the SBs in the tensile samples.

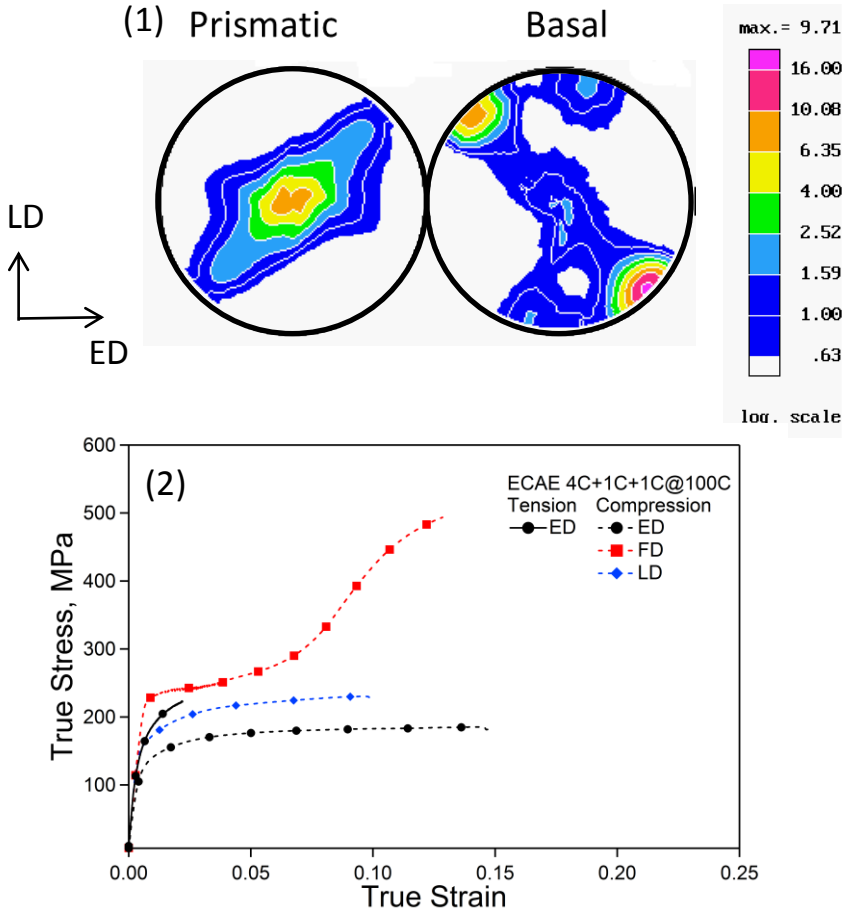

Figure 4.14 (1) Basal and prismatic pole figures and (2) Room temperature mechanical responses of ECAE processed AZ31B alloy processed via 4C+1C+1C@100 °C.

For better understanding the effect of grain size in the strength of the processed alloy, we chose and compared three cases that have similar textures (C texture) but with different grain sizes. The compressive yield strengths (CYS) along FD in 4C and 4C+1C were 143 and 180 MPa, respectively. This value was increased to ~226 MPa (Table 4.4) for 4C+1C+1C@100 °C.

We tried to conduct an additional pass following route A at 100 °C after 4A+1A with the same technique explained for 4C+1C+1C@100 °C, but this attempt was not

successful. The reason for this failure is thought to be that basal planes did not orient favorably along the shear plane of ECAE. In addition, the processing temperature was decreased substantially making the alloy hard to deform. Based on the results given, we came to a conclusion that conducting a pass at a temperature between 150 °C and 100 °C is necessary.

Table 4.4 Compression responses of AZ31B Mg alloy ECAE processed using temperature strep-down method following 4C+1C+1C@100 °C.

Billet	Direction	Compression	
		0.2% proof stress (MPa)	UTS (MPa)
4C+1C+1C@100 °C	ED	128.35 ±2.83	189.55 ±5.88
	LD	152.31 ±4.79	218.18 ±17.3
	FD	225.75 ±1.13	485.34 ±11

We lowered the processing temperature for only 25 °C after the fifth pass, to have a crack-free billet. Based on the previous results, 4C+1C and 4A+1C were good candidates to apply more ECAE passes on them. This additional pass was applied followed by a 180° rotation around ED at 125 °C. Back pressure was increased to 70 MPa and extrusion rate was decreased to 0.038 mm/s, as the reason was explained in

section 3.2. These two cases are called 4C+1C+1C (note the difference between labeling this case and 4C+1C+1C@100 °C case) and 4A+1C+1C, respectively.

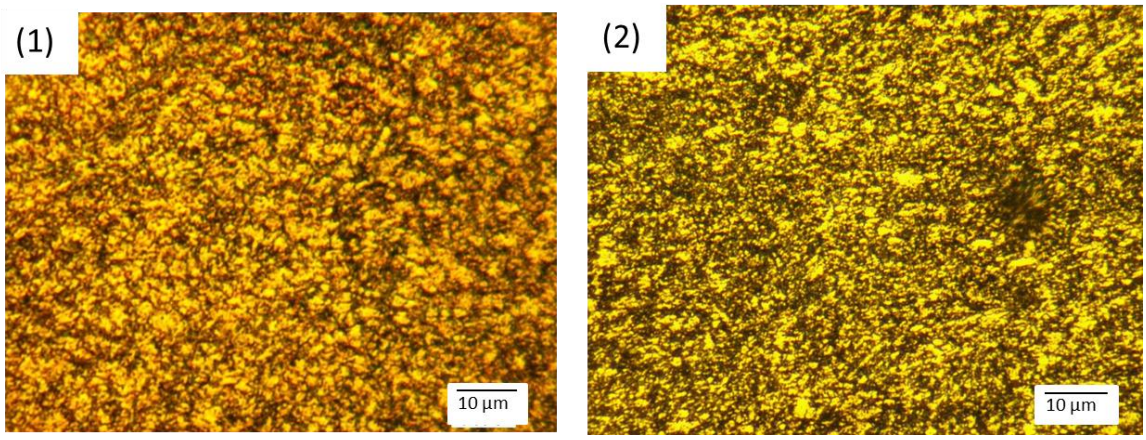

Figure 4.15 Optical micrographs of AZ31B ECAE samples processed by (1) 4C+1C+1C, (2) 4A+1C+1C.

Figure 4.15 shows the microstructure of the two processed samples. The grain size was reduced to nano scale and the grain size distribution seems to be uniform for both cases. Optical microscopy is not a good technique for measuring the grain size at nano scales, but it gives a good image of grain morphology. Thus, SEM and TEM were carried out for the 4A+1C+1C case, for measuring the grain size, shown in Figure 4.16. The grain size distribution (Figure 4.16 (3)) shows a homogenized structure and the grain size was significantly reduced to ~370 nm, measured by SEM. From TEM observations, an average grain size of ~340 nm was measured, which is comparable with what was obtained from SEM. A high dislocation density was seen all through the sample, but no twinning was observed.

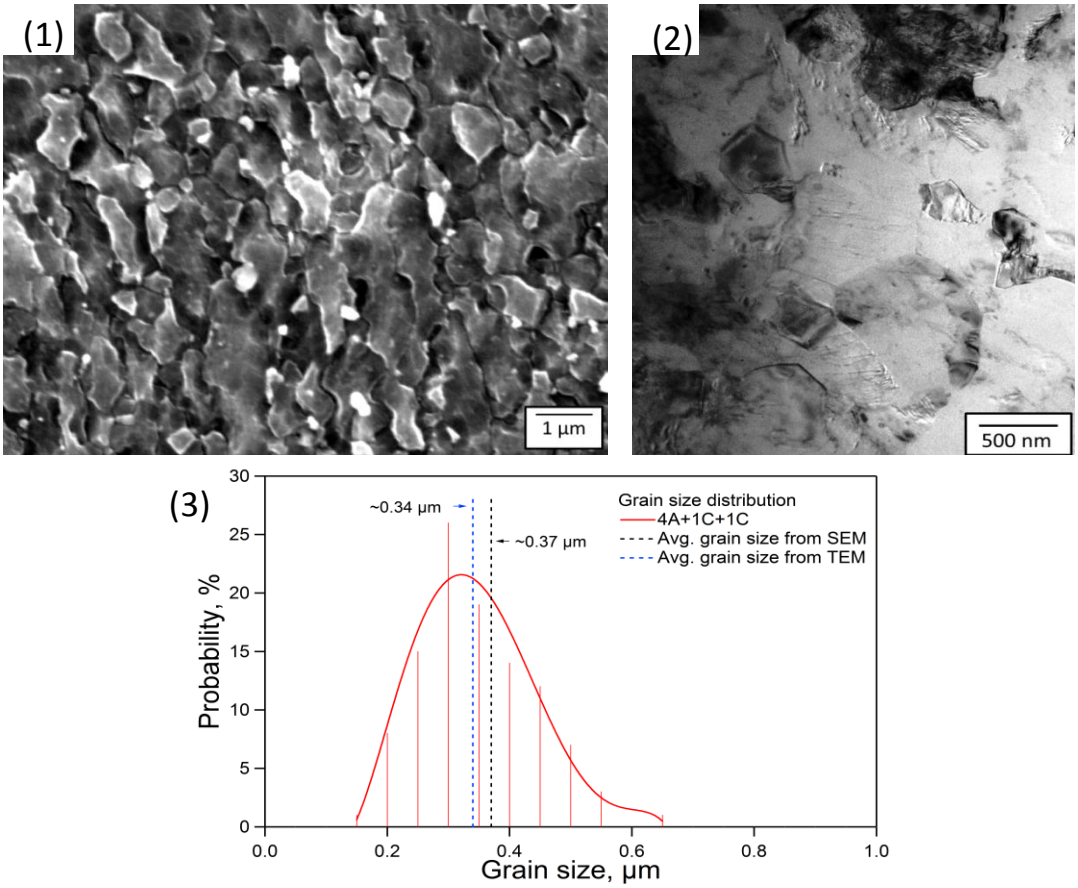

Figure 4.16 (1) Secondary electron image, (2) Transmission electron micrograph and (3) Grain size distribution of UFG AZ31B, processed via hybrid route 4A+1C+1C.

Figure 4.17 (1) shows the (0002) and $(10\bar{1}0)$ pole figures of 4C+1C+1C, which resemble the "C" texture, having a strong basal peak 45° away from LD. It can be argued that the continuation of conducting only C routes will result in only a 45° single basal peak which is greatly favorable to shear by its basal planes during ECAE. When the basal activity increases, the tensile yield strength decreases. Thus, this texture tends to be very soft along ED and LD. However, a highly oriented 45^{o} basal texture will be particularly suited to applications where severe strength anisotropy will be beneficial.

The 4A+1C+1C texture can be categorized as "A+C" texture (Figure 4.17 (2)) and we expect to activate the same deformation mechanisms in tension and compression as were seen in this type of group.

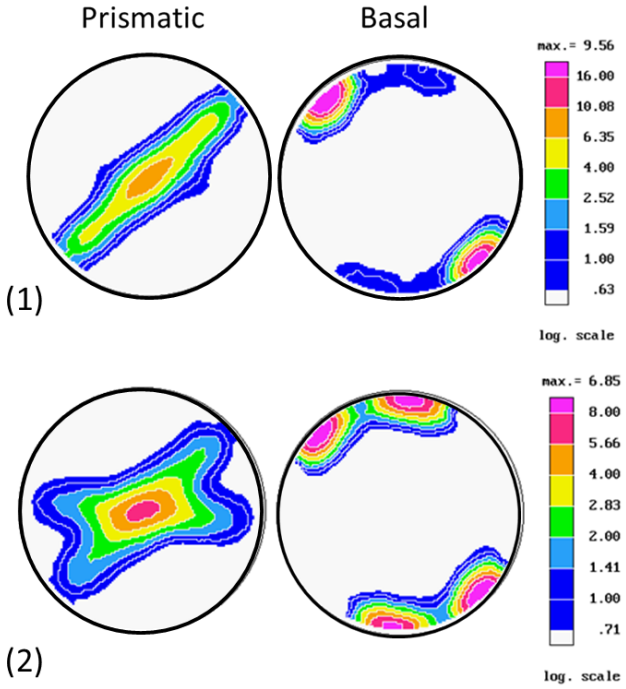

Figure 4.17 (0002) and $(10\bar{1}0)$ pole figures of (1) 4C+1C+1C and (2) 4A+1C+1C.

The mechanical responses of the two hybrid cases (4C+1C+1C, 4A+1C+1C) in tension and compression are shown in Figure 4.18. The first observation from these curves is the improvement in tensile yield strength (TYS) along FD, especially in the 4A+1C+1C case. To the best of the author's knowledge the TYS of 384 MPa (Table 4.5) for 4A+1C+1C is the highest TYS reported for the AZ31B alloy so far. This high strength was achieved without sacrificing ductility. As expected for the "A+C" texture, low ductility was seen for ED tension and LD compression, due to the activation of

compressive twins. The intensity of the secondary basal peak and its location in the basal pole figure can significantly influence the slip activities during ECAE, and hence, the evolving texture. The different compressive and tensile responses along ED and LD for the two cases are the consequences of the location of that secondary basal peak.

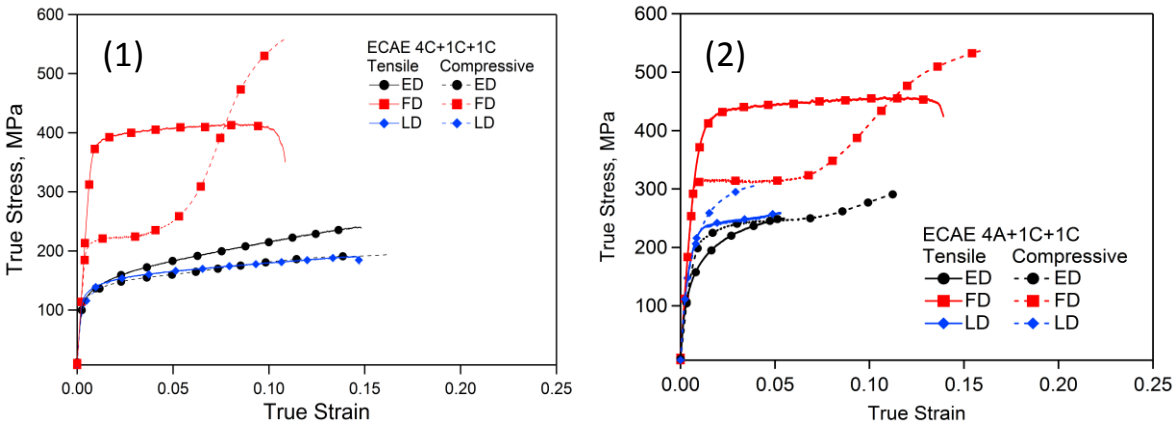

Figure 4.18 Room temperature true tensile and compressive responses of AZ31B alloy ECAE samples processed via (1) 4C+1C+1C and (2) 4A+1C+1C.

After conducting a successful pass at 125 °C and investigating the effect of this processing on grain refinement and mechanical properties, we found that 4A+1C+1C gives us better results in general.

The last processing case was designed to investigate the effect of combining routes A and C at low temperature processing. We predicted that an additional pass following the C route would soften the billet. Thus, one more ECAE pass without rotation was conducted on 4A+1C+1C at 125 °C, with back pressure of 80 MPa and an extrusion rate of 0.038 mm/s, which would be called 4A+1C+1C+1A. We chose the same processing temperature as its previous pass to see if applying multiple passes at a

certain processing temperature (less than 200 °C) would enhance the strength and reduce the grain size noticeably. Typically, decreasing the processing temperature for every additional pass increases the chances of failure while extruding.

Table 4.5 Tension and compression responses of AZ31B Mg alloy ECAE processed using temperature strep-down method following 4C+1C+1C and 4A+1C+1C.

Billet	Direction	Tension		Compression	
		0.2% proof stress (MPa)	UTS (MPa)	0.2% proof stress (MPa)	UTS (MPa)
4C+1C+1C	ED	125.9 ±4.10	236.58 ±6.25	120.96 ±2.49	183.67 ±14
	LD	129.55 ±0.8	191.28 ±0.6	110.7 ±5.59	148.25 ±1.87
	FD	369.45 ±5.38	409.3 ±9.19	208.87 ±2.75	559.79 ±1.76
4A+1C+1C	ED	136.19 ±3	249.05 ±0.98	195.14 ±7.81	289.63 ±1.47
	LD	204 ±0.8	259.67 ±0.2	198.18 ±8.48	317.52 ±12.14
	FD	384.36 ±6.39	455.3 ±3.53	303.04 ±10.3	536.66 ±0.23

Figure 4.19 shows the grain morphology of this case. Obviously, having ECAE processed the billet for a total of seven passes; we expect really fine grains in 4A+1C+1C+1A.

Figure 4.20 (1) shows the basal and prismatic pole figures of the 4A+1C+1C+1A samples from the flow plane of the billet. Since the last pass was followed by route A,

the two basal peaks in 4A+1C+1C, got closer (as seen in “A” type texture) in this new case.

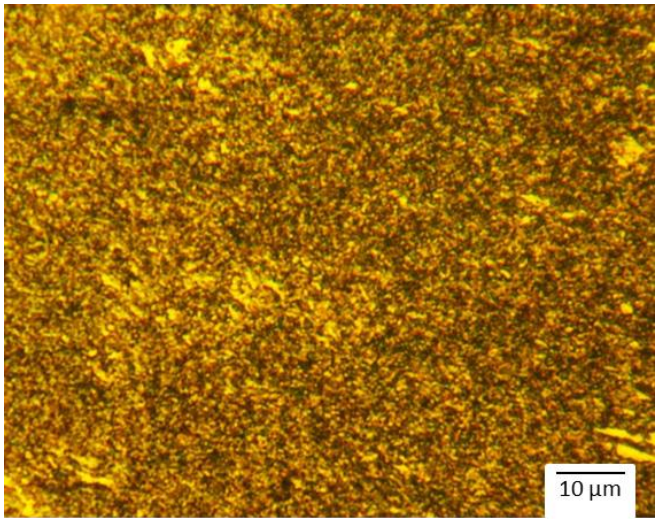

Figure 4.19 Optical micrograph of AZ31B ECAE processed via a seven-pass hybrid route called 4A+1C+1C+1A.

The mechanical responses along the three orthogonal directions shown in Figure 4.20 (2) seem not to be improved (especially in FD tension, the yield strength was even decreased) compared to 4A+1C+1C case. Low ductility was seen along ED tension and LD compression due to the activation of compressive twins. On the contrary, for ED compression and LD tension tensile twining was activated. Table 4.6 lists the YS and UTS along ED, FD and LD for 4A+1C+1C+1A.

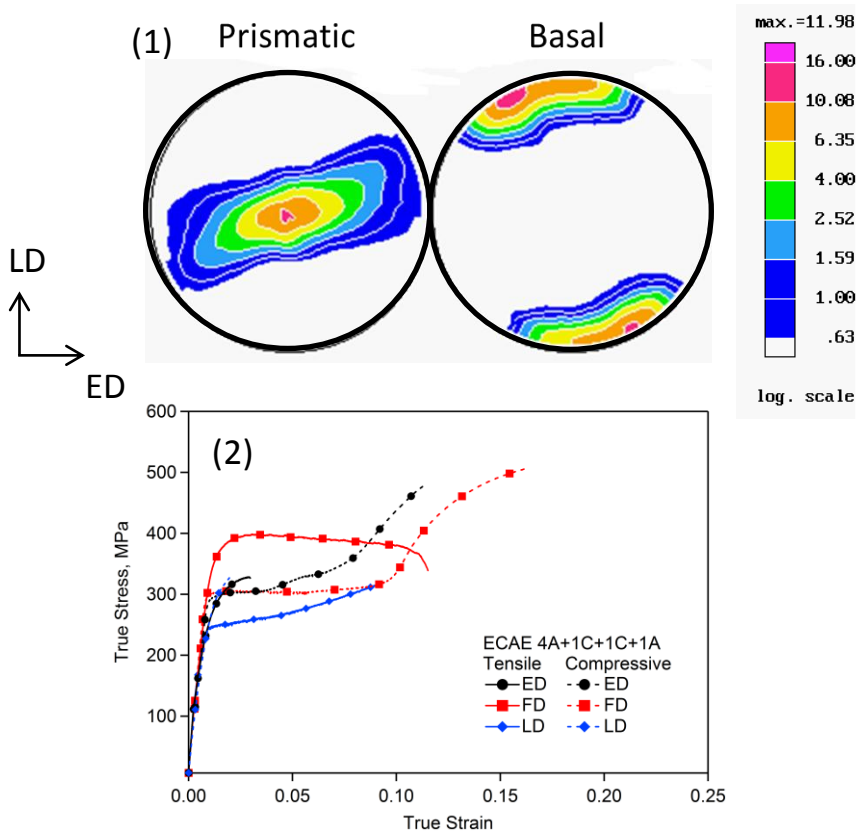

Figure 4.20 (1) Basal and prismatic pole figures and (2) Room temperature mechanical responses of ECAE processed AZ31B alloy processed via 4A+1C+1C+1A.

Table 4.6 Mechanical responses of AZ31B Mg alloy ECAE processed using temperature strep-down method following 4A+1C+1C+1A.

Billet	Direction	Tension		Compression	
		0.2% proof stress (MPa)	UTS (MPa)	0.2% proof stress (MPa)	UTS (MPa)
4A+1C+1C+1A	ED	273.91 ±0.98	318.97 ±13.34	292.4 ±1.41	365.65 ±24.5
	LD	241.26 ±3.05	314.47 ±3.11	288.21 ±9.85	326.16 ±4.92
	FD	354.35 ±1.2	398.81 ±0.11	300.73 ±4.64	516.67 ±16.02

Further ECAE processing at lower temperatures of the AZ31B alloy was investigated. An additional pass at 125 °C was conducted with a 180° rotation after 4A+1C, 4C+1C. For better visualizing our improvement in mechanical properties of AZ31B Mg alloy and also see where we stand compared to the literature, Figure 4.21 is shown which shows the specific strength vs. elongation to failure for typical structural aluminum alloys [89] and steels [90, 91] and magnesium alloys [2, 36, 54, 70]. As can be seen, the highest specific strength goes to letter Z which is FD tension for 4A+1C+1C hybrid route.

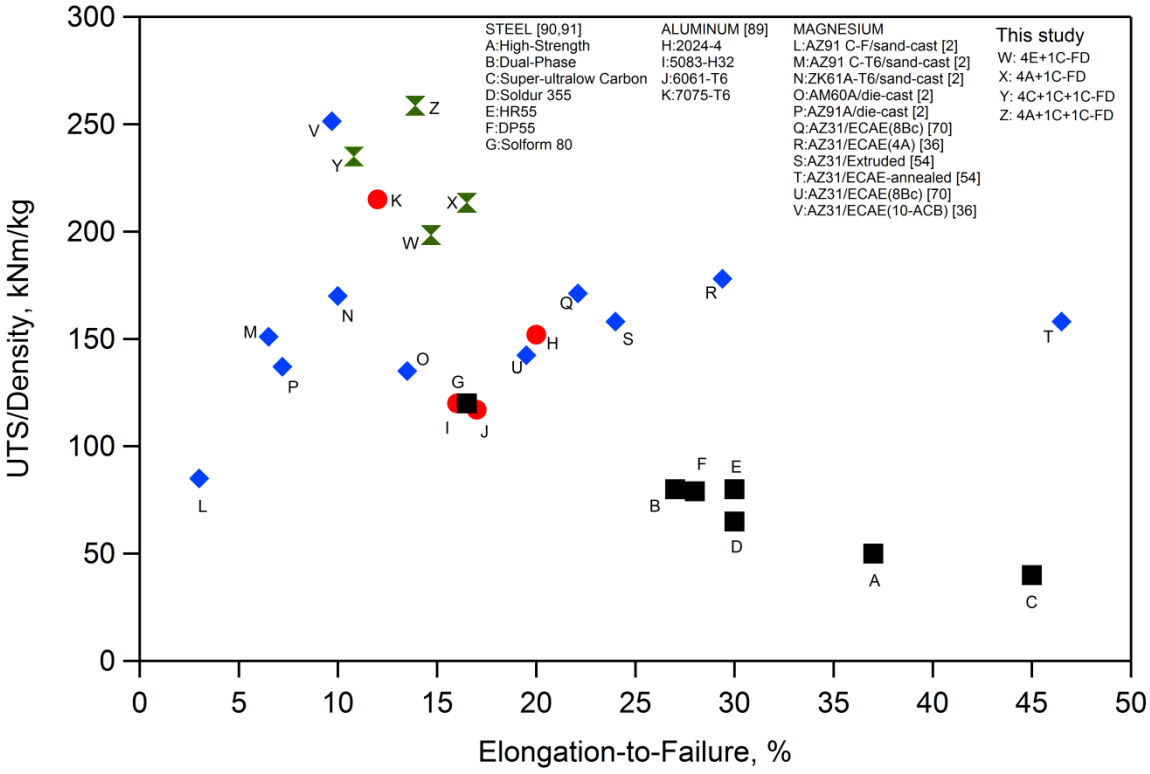

Figure 4.21 Specific strength-ductility balance in some of the ECAE processed AZ31B alloys studied in this thesis. Included are the data for typical structural aluminum alloys [89] and steels [90, 91] and magnesium alloys [2, 36, 54, 70].

The findings of this research are summarized here:

1. The alloy processed at the lower temperature reveals more homogenous microstructure.
2. Encapsulating the billet did not seem to be a good technique to ECAE process at low temperatures. Either another type of metal can should be chosen or the IF steel can should be strengthened before encapsulation. However, the billet could be ECAE processed without the encapsulation method.
3. The present results clearly show that twins are formed in UFG Mg having a grain size as small as 370 nm, which is much smaller than the critical grain size reported in the literature [92].

4.4 Grain Size Hardening on Different Deformation Mechanisms

There were a lot of studies focusing on the dependence of the flow stresses on grain sizes in Mg alloys, which found that the Hall-Petch relation can be applied to it [47, 93-96] . But, to the best of the authors' knowledge, Hall-Petch effect for individual deformation systems on AZ31B alloy has not been investigated. The present research is an effort to investigate the effect of grain size on the basal slip, prismatic slip and tensile twinning in the AZ31B alloy at room temperature.

First we focus on the grain size hardening of prismatic slip. We need to make sure that mainly prismatic slip gets activated during deformation. It was previously emphasized that when the c-axis is constrained, prismatic slip is expected to be favorable. According to Figure 4.21, Al-Maharbi [61] showed the predicted relative

activities during tension along FD of the ECAE processed AZ31B Mg samples up to four passes following route A (4A case), which matches the statement above.

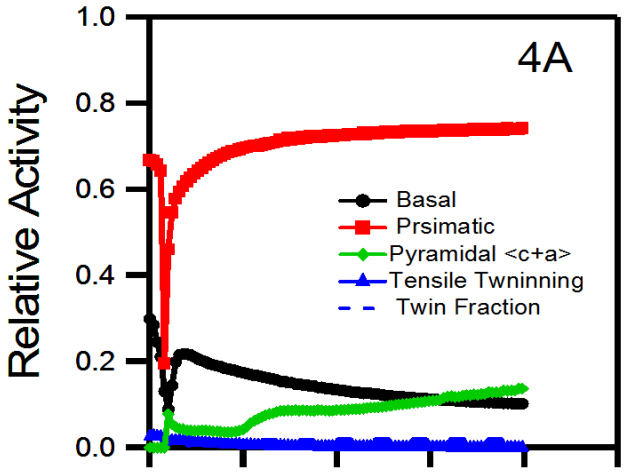

Figure 4.22 The predicted relative activities of deformation modes during tension along the FD of the AZ31B ECAE processed up to four passes following route A (4A) [61].

4A, 4A+1C and 4A+1C+1C cases were chosen because they all share the same "A+C" texture but with different grain sizes. For better comparison, their grain size distributions are depicted in Figure 4.22. By applying tension along FD for all of them, we expect prismatic slip to be activated.

True stress–true strain curves shown in Figure 4.23 (1) are for all processed samples tested at room temperature in tension along the FD with varying grain sizes up to the breaking point. The ductility does not seem to be affected by the change in the grain size. As anticipated, the flow stress decreases with increasing grain size. This shows that reduction in grain size hardens the prismatic slip. Hall–Petch plot is presented in Figure 4.23 (2) for the 0.2% offset proof stress, $\sigma_{0.002}$. Using the standard relation:

$$\sigma_y = \sigma_0 + k_y d^{-1/2}$$

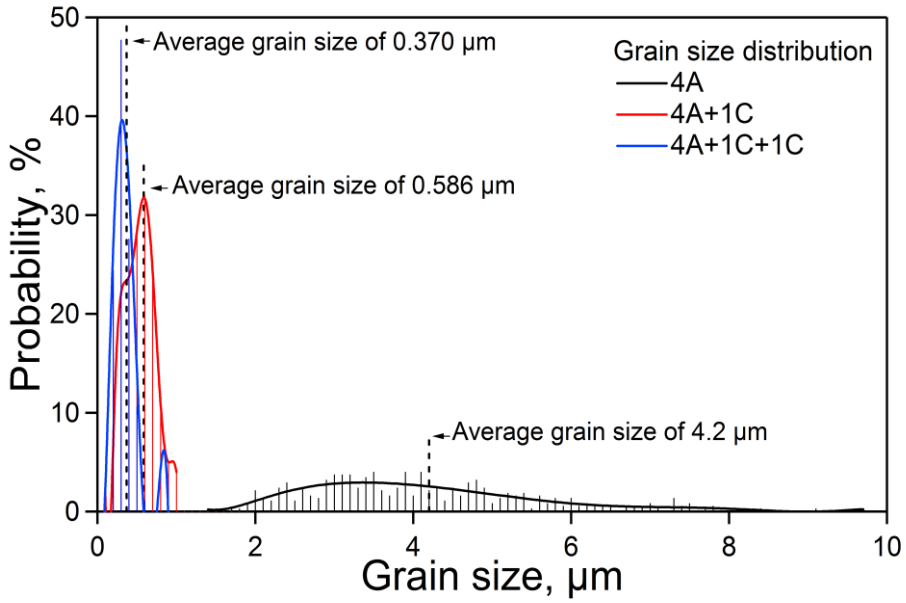

Figure 4.23 Grain size distribution of 4A, 4A+1C and 4A+1C+1C.

where σ_y is the yield stress, σ_0 is the friction stress, d is the grain size, and k_y is the characteristic constant representing the resistance to dislocation motion provided by the grain boundaries. The Hall-Petch slope is in agreement with earlier observations of Jain et al. [47], Del Valle et al. [93] for AZ31B Mg alloy with the same texture and at micron scale grain sizes. Thus we could draw a line passing from all the cases having grain sizes more than 1 μm. As the grain size decreased to nano scale, the Hall-Petch slope seemed to change. Thus, more work needs to be done to understand this difference in slope.

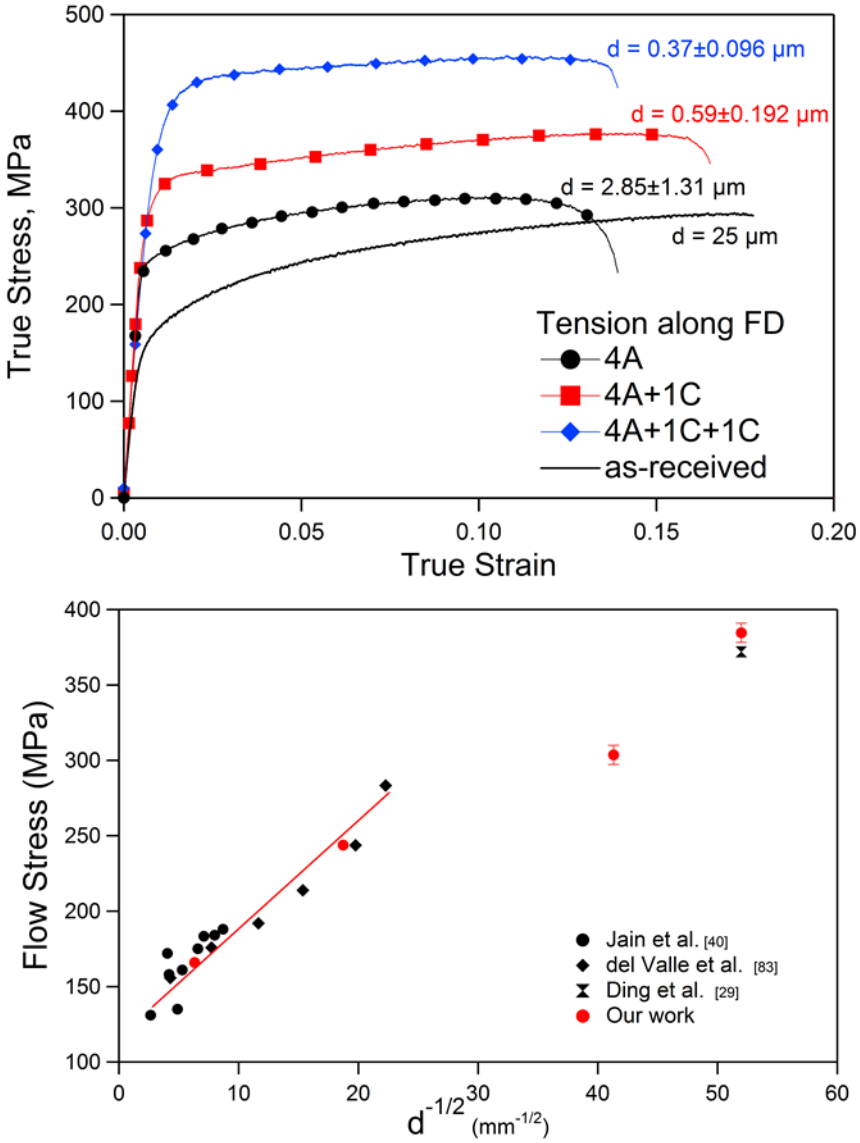

Figure 4.24 (1) Room temperature true stress vs. strain curves for samples of different grain sizes having "A+C" texture tested in tension along FD activating prismatic slip (2) Schematic of the present interpretation of a Hall-Petch plot seen for yielding controlled by prismatic slip.

The activation of tensile twinning is easy to distinguish in the stress-strain curve showing a plateau region with nearly zero work hardening rate. This time we chose cases from the "C" texture group. By applying compression along FD (c-axis compression)

tensile twinning was activated. Figure 4.24 depicts the increase in the flow stress by grain refinement. According to a recent study by Lee et al. [83], they observed that the strain range for the plateau region increases with decreasing grain size. However, we observed the opposite behavior; as the grain size reduced, less number of grains twinned.

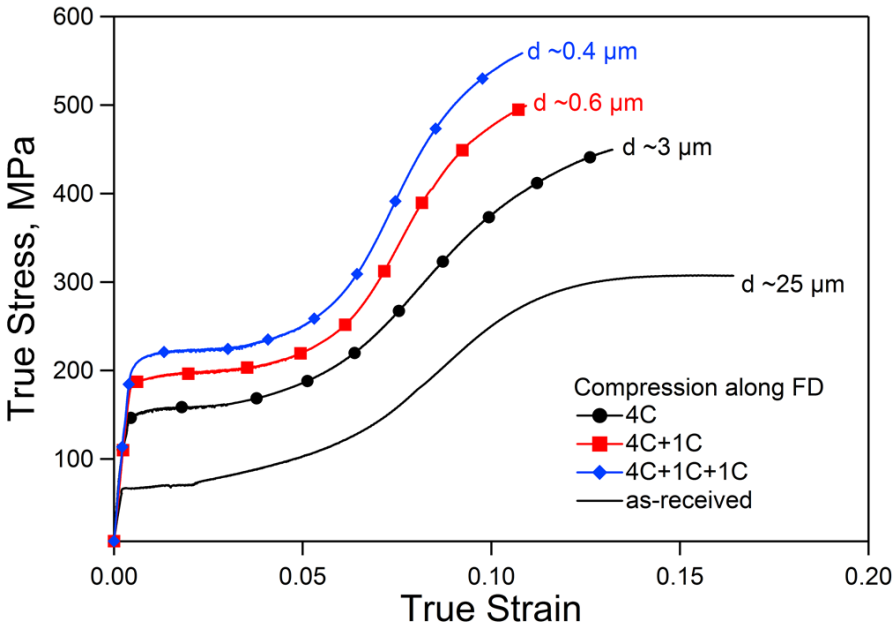

Figure 4.25 Room temperature true stress vs. strain curves for processed samples of different grain sizes having "C" texture tested in compression along FD activating tensile twinning.

As mentioned several times throughout this thesis, having a high Schmid factor for grain orientations favors basal slip to operate. Applying tension along ED for cases with "C" texture, results in basal slip. According to Figure 4.25, basal slip does not harden as much as prismatic and tensile twinning.

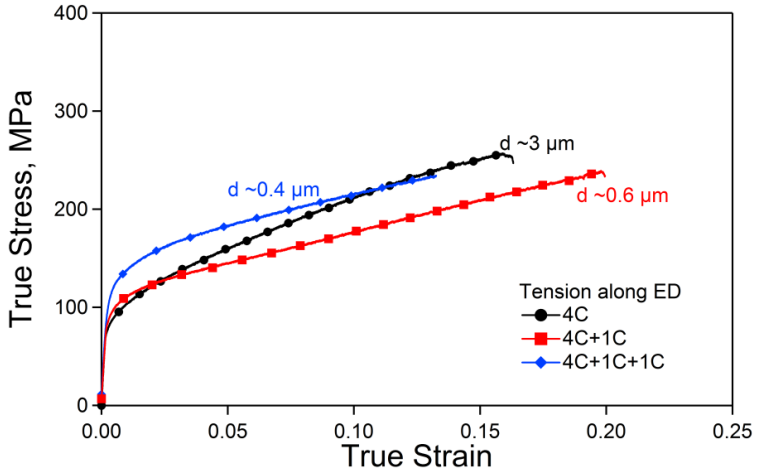

Figure 4.26 Room temperature true stress vs. strain curves for processed samples of different grain sizes having "C" texture tested in tension along ED activating basal slip.

An investigation on the grain size hardening behavior of different deformation mechanisms was performed. A summary of the results is depicted in Figure 4.26. The Hall-Petch constant for Basal slip was much smaller than prismatic slip and tensile twinning. Achieving a very high yield strength is promising by activating only prismatic slip for finer grains.

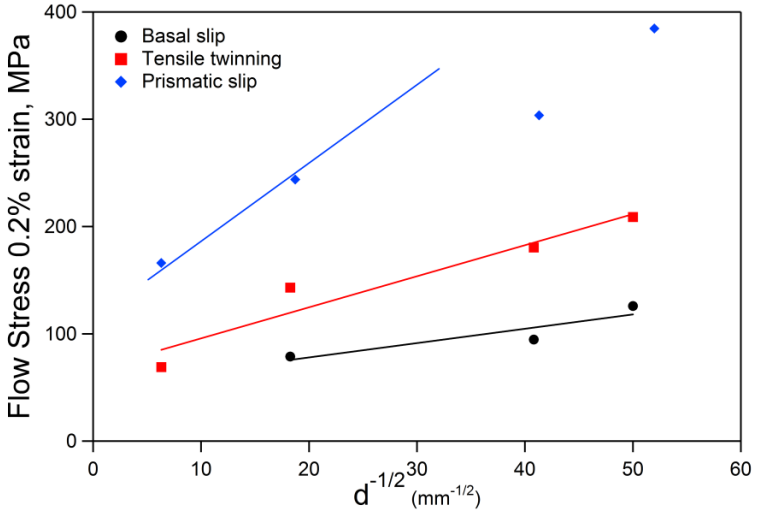

Figure 4.27 Hall-Petch plots of the flow stress at 0.2% strain for basal slip, prismatic slip and tensile twinning.

CHAPTER V

CONCLUSIONS

Equal channel angular extrusion (ECAE) process was shown to be very beneficial in introducing a wide variety of crystallographic texture, and grain sizes on AZ31B Mg alloy by varying the processing temperatures, processing routes, number of passes, and their combinations. The influence of the crystallographic texture on the formability of AZ31B Mg alloy as well as the effect of the grain size hardening on different deformation mechanisms were investigated.

The main findings can be summarized as follows:

1. The flow stress anisotropy and tension/compression (T/C) asymmetry of AZ31B Mg alloy depend on the orientation of the basal poles with respect to the testing directions. The more the distribution of the basal poles is spread, the lower the flow anisotropy and T/C asymmetry are.
2. The activity of twins is responsible for the T/C asymmetry in AZ31B Mg alloy. Moreover, the activity of different slip and twinning systems and strong basal textures are the main reasons behind the flow stress anisotropy in these alloys. Stronger basal textures lead to the activity of twinning upon loading along certain directions and under certain type of loading (compression or tension).
3. ECAE deformation produces different textures in AZ31B Mg samples. These textures can be classified in four categories that are called Texture A, Texture C Texture A+C and Texture B_C. “A” texture has a single spread peak on the basal

texture plot of the flow plane which is almost parallel to the longitudinal direction (LD). Texture "C" has two basal peaks separated by 60-65° on the flow plane that one of them makes an angle of about 45° from LD, counterclockwise (CCW) and is more intense than the other peak. Texture "A+C" has two basal peaks close to each other, one almost parallel to LD and the other close to 45° from LD. Or it can be a single peak spanning from 0° to 45° (CCW) from LD. At last, in texture "B_C" basal poles are aligned along a pole making an angle of about 27-38° from LD.

4. A high strength/high ductility AZ31B alloy was achieved by multiple-temperature equal channel angular extrusion processing, starting at 200 °C for the first four passes to get advantage of softening through dynamic recrystallization (DRX) and then performing additional passes at lower temperatures down to 125 °C following a combination of routes A and C, to suppress DRX and grain growth. The specific strength (ultimate tensile strength divided by the density)-ductility balance obtained in some cases of this work is notably better than what is reported in the literature for Mg alloys and conventional Al alloys and steels.
5. Grain size hardening of prismatic slip and tensile twinning seems to be very pronounced. On the other hand, basal slip showed a small hardening as the grain size was reduced.

CHAPTER VI

SUGGESTIONS FOR FUTURE WORKS

There are some ideas for future work that can be summarized as follows:

1. Decreasing the processing temperature for every additional pass increases the chances of failure while extruding. The grain refinement after conducting several ECAE passes at 150 °C after the high temperature processing can be comparable/or even better to the cases which underwent two ECAE passes at 150 °C and 125 °C. Thus, the effect of higher number of passes at 100 °C should be interesting too.
2. A more detailed investigation must be conducted on the activity of compressive twinning in the ultrafine-grained AZ31B Mg alloy at room temperature, since the low ductility seems to be more affected from the activation of this mechanism.
3. Annealing heat treatments of low temperature ECAE processed samples should enhance the ductility appreciably without much sacrifice in the strength.
4. Post-ECAE processing can be used to further increase the strength of Mg alloys. Low temperature rolling is a good candidate to further refine the grains and strain hardens the alloy. Compressing the ECAE processed billets that have Texture A type along their extrusion axis can introduce twinning in the billet which increases the volume fraction of boundaries that hinder the dislocation movement. This is expected to have significant increase on yield strength of the alloy, especially along FD.

5. In this study, we only focused on getting high flow stress anisotropy. One can try to apply B_C route at low temperatures to create more spread texture and getting more isotropic behavior. As a result higher yield strengths would be achieved along the three directions.
6. The effect of strain rate on different deformation mechanisms needs to be investigated. For example, knowing the difference in strain rate sensitivity of deformation systems is helpful.

REFERENCES

[1] B.L. Mordike, T. Ebert, Mat. Sci. Eng. A 302 (2001) 37.

[2] M.M. Avedesian, H. Baker, Magnesium and Magnesium Alloys, ASM Specialty International, Materials Park, Ohio, 1999.

[3] K. Mathis, J. Gubicza, N.H. Nam, J. Alloy Compd. 394 (2005) 194.

[4] X.M. Feng, T.T. Ai, T. Nonferr. Metal Soc. 19 (2009) 29.

[5] S. Kleiner, P.J. Uggowitzer, Mat. Sci. Eng A 379 (2004) 258.

[6] J. Koike, Metall. Mater. Trans. A 36A (2005) 1689.

[7] T. Al-Samman, G. Gottstein, Mat. Sci. Eng. A 490 (2008) 411.

[8] H. Watanabe, T. Mukai, K. Ishikawa, J. Mater. Sci. 39 (2004) 1477.

[9] H.K. Lin, J.C. Huang, Mater. Trans. 43 (2002) 2424.

[10] V.V. Stolyarov, R.Z. Valiev, Advances in Nanocrystallization 307 (1999) 185.

[11] V.M. Segal, Mat. Sci. Eng. A 271 (1999) 322.

[12] V.M. Segal, Mat. Sci. Eng. A 197 (1995) 157.

[13] R.Z. Valiev, T.G. Langdon, Prog. Mater. Sci. 51 (2006) 881.

[14] T.G. Langdon, Mat. Sci. Eng. A 462 (2007) 3.

[15] I.J. Beyerlein, L.S. Toth, Prog. Mater. Sci. 54 (2009) 427.

[16] I.J. Beyerlein, C.N. Tome, Mat. Sci. Eng. A 380 (2004) 171.

[17] R.Z. Valiev, R.K. Islamgaliev, I.V. Alexandrov, Prog. Mater. Sci. 45 (2000) 103.

[18] S. Li, I.J. Beyerlein, M.A.M. Bourke, Mat. Sci. Eng. A 394 (2005) 66.

[19] S.Y. Li, I.J. Beyerlein, C.T. Necker, Acta. Mater. 54 (2006) 1397.

[20] S.R. Agnew, P. Mehrotra, T.M. Lillo, G.M. Stoica, P.K. Liaw, Mat. Sci. Eng. A 408 (2005) 72.

[21] S. Ferrasse, V.M. Segal, S.R. Kalidindi, F. Alford, Mat. Sci. Eng. A 368 (2004) 28.

[22] I.J. Beyerlein, R.A. Lebensohn, C.N. Tome, Mat. Sci. Eng. A 345 (2003) 122.

[23] A. Gholinia, P. Bate, P.B. Prangnell, Acta Mater. 50 (2002) 2121.

[24] P.B. Berbon, M. Furukawa, Z. Horita, M. Nemoto, T.G. Langdon, Metall. Mater. A 30 (1999) 1989.

[25] M.W. Fu, M.S. Yong, Q. Pei, H.H. Hng, Mater. Manuf. Process 21 (2006) 507.

[26] Z. Horita, M. Furukawa, M. Nemoto, T.G. Langdon, Mater. Sci. Tech. Ser. 16 (2000) 1239.

[27] M. Furukawa, Z. Horita, T.G. Langdon, Mat. Sci. Eng. A 332 (2002) 97.

[28] Y. Iwahashi, Z. Horita, M. Nemoto, T.G. Langdon, Acta Mater. 46 (1998) 3317.

[29] R.E. Barber, T. Dudo, P.B. Yasskin, K.T. Hartwig, Scripta Mater. 51 (2004) 373.

[30] J.R. Bowen, P.B. Prangnell, F.J. Humphreys, Mater. Sci. Tech. Ser. 16 (2000) 1246.

[31] H.S. Kim, M.H. Seo, S.I. Hong, Mat. Sci. Eng. A 291 (2000) 86.

[32] R.E. Goforth, K.T. Hartwig, L.R. Cornwell, Nato. Sci. S Prt 3 Hi. 80 (2000) 3.

[33] Y. Iwahashi, J.T. Wang, Z. Horita, M. Nemoto, T.G. Langdon, Scripta Mater. 35 (1996) 143.

[34] K. Nakashima, Z. Horita, M. Nemoto, T.G. Langdon, Acta Mater. 46 (1998) 1589.

[35] S.R. Agnew, J.A. Horton, T.M. Lillo, D.W. Brown, Scripta Mater. 50 (2004) 377.

[36] S.X. Ding, W.T. Lee, C.P. Chang, L.W. Chang, P.W. Kao, Scripta Mater. 59 (2008) 1006.

[37] V.M. Segal, Mat. Sci. Eng. A 345 (2003) 36.

[38] S.Y. Li, A.A. Gazder, I.J. Beyerlein, E.V. Pereloma, C.H.J. Davies, Acta Mater. 54 (2006) 1087.

[39] C.S. Roberts, Magnesium and Its Alloys, Wiley, New York, 1960.

[40] G.I. Taylor, J. I. Met., 62 (1938) 307.

[41] R. Von Mises, Math. Mech. 6 (1928) 85.

[42] M.H. Yoo, Metall. A 12 (1981) 409.

[43] J.F. Stohr, J.P. Poirier, Philos. Mag. 25 (1972) 1313.

[44] H. Yoshinaga, R. Horiuchi, T. Jpn I. Met. 5 (1964) 14.

[45] S. Graff, W. Brocks, D. Steglich, Int. J. Plast. 23 (2007) 1957.

[46] S.R. Agnew, O. Duygulu, Magnesium Alloys 2003, Pts 1 and 2, 419-4 (2003) 177.

[47] A. Jain, O. Duygulu, D.W. Brown, C.N. Tome, S.R. Agnew, Mat. Sci. Eng. A 486 (2008) 545.

[48] L. Wu, A. Jain, D.W. Brown, G.M. Stoica, S.R. Agnew, B. Clausen, D.E. Fielden, P.K. Liaw, Acta Mater. 56 (2008) 688.

[49] J. Koike, T. Kobayashi, T. Mukai, H. Watanabe, M. Suzuki, K. Maruyama, K. Higashi, Acta Mater. 51 (2003) 2055.

[50] S.H. Choi, E.J. Shin, B.S. Seong, Acta Mater. 55 (2007) 4181.

[51] G.G. Yapici, I.J. Beyerlein, I. Karaman, C.N. Tome, Acta Mater. 55 (2007) 4603.

[52] D.J. Alexander, I.J. Beyerlein, Mat. Sci. Eng. A 410 (2005) 480.

[53] G.G. Yapici, I.J. Beyerlein, C.N. Tome, I. Karaman, S.C. Vogel, C. Liu, Acta Mater. 57 (2009) 4855.

[54] T. Mukai, M. Yamanoi, H. Watanabe, K. Higashi, Scripta Mater. 45 (2001) 89.

[55] A. Yamashita, Z. Horita, T.G. Langdon, Mat. Sci. A 300 (2001) 142.

[56] Z. Horita, T. Fujinami, T.G. Langdon, Mat. Sci. Eng. A 318 (2001) 34.

[57] V.V. Stolyarov, Y.T. Zhu, I.V. Alexandrov, T.C. Lowe, R.Z. Valiev, Mat. Sci. Eng. A 299 (2001) 59.

[58] R.B. Figueiredo, Z. Szaraz, Z. Trojanova, P. Lukac, T.G. Langdon, Scripta Mater. 63 (2010) 504.

[59] H.K. Kim, W.J. Kim, Mat. Sci. Eng. A 385 (2004) 300.

[60] J.F. Jiang, Y. Wang, Z.M. Du, J.J. Qu, Y. Sun, S.J. Luo, J. Mater. Process Tech. 210 (2010) 751.

[61] M. Al-Maharbi, PhD dissertation, Texas A&M University (2009).

[62] S.R. Agnew, P. Mehrotra, T.M. Lillo, G.M. Stoica, P.K. Liaw, Acta Mater. 53 (2005) 3135.

[63] M. Mabuchi, H. Iwasaki, K. Yanase, K. Higashi, Scripta Mater. 36 (1997) 681.

[64] W.J. Kim, C.W. An, Y.S. Kim, S.I. Hong, Scripta Mater. 47 (2002) 39.

[65] Y.V.R.K. Prasad, N. Ravichandran, B. Mater. Sci. 14 (1991) 1241.

[66] A. Galiyev, R. Kaibyshev, G. Gottstein, Acta Mater. 49 (2001) 1199.

[67] S. Biswas, S.S. Dhinwal, S. Suwas, Acta Mater. 58 (2010) 3247.

[68] A.E. Smith, Surf. Sci. 601 (2007) 5762.

[69] L. Jin, D.L. Lin, D.L. Mao, X.Q. Zeng, W.J. Ding, Mater. Lett. 59 (2005) 2267.

[70] K. Xia, J.T. Wang, X. Wu, G. Chen, M. Gurvan, Mat. Sci. Eng. A 410 (2005) 324.

[71] W.J. Kim, H.T. Jeong, Mater. Trans. 46 (2005) 251.

[72] M. Al-Maharbi, I. Karaman, I.J. Beyerlein, D.C. Foley, K.T. Hartwig, L. Kecskes, S. Mathaudhu, Mat. Sci. Eng. A 528 (2011) 7616.

[73] D.C. Foley, M. Al-Maharbi, K.T. Hartwig, I. Karaman, L.J. Kecskes, S.N. Mathaudhu, Scripta Mater. 64 (2011) 193.

[74] S.R. Agnew, C.N. Tome, D.W. Brown, T.M. Holden, S.C. Vogel, Scripta Mater. 48 (2003) 1003.

[75] M.R. Barnett, Mat. Sci. Eng. A 464 (2007) 8.

[76] S.V. Harren, H.E. Deve, R.J. Asaro, Acta Metall Mater. 36 (1988) 2435.

[77] M. Al-Maharbi, D. Foley, I. Karaman, I. Beyerlein, K.T. Hartwig, L.J. Kecskes, S. Mathaudhu, Magnesium Technology 2010, TMS Warrendale, PA, 2010, p. 445.

[78] D.L. Lin, L. Jin, D.L. Mao, X.Q. Zeng, B. Chen, Mat. Sci. Eng. A 423 (2006) 247.

[79] P.L. Sun, P.W. Kao, C.P. Chang, Metall. Mater. A 35 (2004) 1359.

[80] G. Proust, C.N. Tomé, A. Jain, S.R. Agnew, Int. J. Plast. 25 (2009) 861.

[81] M.R. Barnett, Z. Keshavarz, X. Ma, Metall. Mater. A 37 (2006) 2283.

[82] M.R. Barnett, Metall. Mater. A 34 (2003) 1799.

[83] W.T. Lee, S.X. Ding, D.K. Sun, C.I. Hsiao, C.P. Chang, L. Chang, P.W. Kao, Metall. Mater. A 42 (2011) 2909.

[84] L. Capolungo, I.J. Beyerlein, C.N. Tome, Scripta Mater. 60 (2009) 32.

[85] P. Cizek, M.R. Barnett, Scripta Mater. 59 (2008) 959.

[86] N. Stanford, M. Barnett, Scripta Mater. 58 (2008) 179.

[87] A. Chapuis, J.H. Driver, Acta Mater. 59 (2011) 1986.

[88] R. Lapovok, L.S. Toth, A. Molinari, Y. Estrin, J. Mech. Phys. Solids 57 (2009) 122.

[89] Aluminum Handbook, Japan Institute of Light Metals, Japan, 1978, p 26.

[90] W. Bleck, Jom-Journal of the Minerals Metals & Materials Society 48 (1996) 26.

[91] G. Marron, P. Teracher, Jom-Journal of the Minerals Metals & Materials Society, 48 (1996) 16.

[92] Q. Yang, A.K. Ghosh, Acta Mater. 54 (2006) 5147.

[93] J.A. del Valle, F. Carreno, O.A. Ruano, Acta Mater. 54 (2006) 4247.

[94] N. Ono, K. Nakamura, S. Miura, Magnesium Alloys 2003, Pts 1 and 2, Trans. Tech. Publications, Switzerland, 2003, p 195.

[95] F.E. Hauser, P.R. Landon, J.E. Dorn, Trans. Am. Soc. Met. 50 (1958) 856.

[96] Armstrong.Rw, Acta Metall. Mater. 16 (1968) 347.

VITA

Sonia Modarres Razavi was born in Mashhad, Iran. She received her Bachelor of Science degree in Mechanical Engineering from Ferdowsi University of Mashhad in 2008. In December 2011, she received her Master of Science in Mechanical Engineering Department at Texas A&M University in College Station.

Ms. Modarres Razavi may be reached at Mechanical Engineering Department, ENPH, Texas A&M University, College Station, TX, 77843. Her email address is sonim168@yahoo.com.